ENO AND WENO SCHEMES BASED ON UPWIND AND CENTRED TVD FLUXES

V.A. Titarev[1] and E.F. Toro[2]

[1] Department of Mathematics, Faculty of Science,
University of Trento, Trento, Italy,
E-mail: Titarev@science.unitn.it,
Web page: http://www.science.unitn.it/~titarev

[2] Laboratory of Applied Mathematics, Faculty of Engineering,
University of Trento, Trento, Italy,
E-mail: toro@ing.unitn.it,
Web page: http://www.ing.unitn.it/toro

Abstract

Very high order methods, such as ENO/WENO methods [20, 30, 18], Runge-Kutta Discontinuous Galerkin Finite Element Methods [11] and ADER methods [54, 45, 46, 58], use high order (e.g. fifth order) polynomial reconstruction of the solution and a lower (first) order monotone flux as the building block. In this paper we propose to use second order TVD fluxes, instead of first-order monotone fluxes, in the framework of such methods. We apply the principle to the finite-volume ENO, WENO and MPWENO schemes. We call the new improved schemes the ENO-TVD, WENO-TVD and MPWENO-TVD schemes respectively. They include both upwind and centred schemes on non-staggered meshes. Numerical results suggest that our schemes are superior to the original schemes used with first order monotone fluxes. This is especially so for long time evolution problems containing both smooth and non-smooth features.

Key words: upwind, centred, weighted ENO, Godunov, HLLC, WAF flux, FLIC flux, ADER

1. INTRODUCTION

We are concerned with improved very high order methods for solving hyperbolic conservation laws. Hyperbolic conservation laws arise in areas as diverse as compressible gas-dynamics, shallow water flows, turbomachinery, turbulence modelling, weather prediction, plasma modelling, rarefied gas dynamics and many others. Analytical solutions are available only in very few special cases and numerical methods must be used in practical applications. Developing such methods is a formidable task since solutions can contain complex smooth structures interspersed with discontinuities. A successful numerical method should resolve discontinuities with correct positions and sharp non-oscillatory profiles and retain high order of accuracy in smooth regions. According to the classical theorem of Godunov [14] *linear* high order methods cannot achieve this dual task. Over the last twenty five years or so remarkable progress has been made in designing *nonlinear* methods which can circumvent Godunov's theorem by being solution-adaptive. A prominent class of such methods is the class of Total Variation Diminishing (TVD) methods [19, 42]. Pioneering examples include the Godunov-Kolgan scheme [23, 24, 25], SHASTA Flux Corrected Transport (FCT) algorithm [5, 6, 7] and MUSCL-type methods [60, 61, 65, 4, 12]. For a review of the TVD methods see [28, 51].

TVD methods avoid oscillations by locally reverting to first order of accuracy near discontinuities and extrema and are therefore unsuitable for applications involving long time evolution of complex structures, such as in acoustic and compressible turbulence. In these applications extrema are clipped as time evolves and numerical diffusion may become dominant. Uniformly very high order methods, both in time and space, are needed for such applications. State-of-the art very high order methods include the class of essentially non-oscillatory (ENO) [20, 40], weighted essentially non-oscillatory (WENO) [30, 18, 41, 29, 1, 33], monotonicity preserving (MP) [41] and monotonicity preserving weighted essentially non-oscillatory (MPWENO) schemes [1], Runge-Kutta Discontinuous Galerkin (RKDG) Finite Element Methods [9, 10, 11] and the Advection-Diffusion-Reaction (ADER) approach [54, 44, 57, 37, 45, 59, 43]. All of these methods are capable of achieving at least third order of accuracy both in time and space. ENO,WENO, MP, MPWENO and ADER schemes enjoy an additional advantage over other methods: these schemes are essentially non-oscillatory. That is, *to the eye*, the solution is free from spurious oscillations. The key idea in the r^{th} -

order ENO reconstruction procedure used in [20, 40] is to consider r possible stencils covering the given cell (in one space dimension) and to select only one, the smoothest, stencil. The reconstruction polynomial is then built using this selected stencil. The WENO reconstruction [30, 18, 1] takes a convex combination of all r stencils with non-linear solution-adaptive weights. The design of the weights involves local estimates of the smoothness of the solution in each possible stencil so that the reconstruction achieves $(2r-1)^{\text{th}}$ - order of spatial accuracy in smooth regions and emulates the r^{th} - order ENO reconstruction near discontinuities. The MPWENO reconstruction [1] is a combination of increasingly high order (e.g. 9^{th} order) WENO reconstructions and a monotonicity preserving (MP) constraint [41]. The MPWENO schemes are, in general, more expensive and require smaller Courant numbers as compared to ENO and WENO schemes. However, the improvements in accuracy usually more than compensate for the higher computational cost.

In the above-mentioned finite-volume methods the reconstruction polynomials $\mathbf{P}_i(x)$ are different from cell to cell. As a result, at each cell interface $x_{i+1/2}$ between cells i and $i+1$ (in one dimension) the reconstruction produces two different values of the vector pf conservative variables $\mathbf{Q}$, namely the left extrapolated value $\mathbf{Q}^L_{i+1/2} = \mathbf{P}_i(x_{i+1/2})$ and the right extrapolated value $\mathbf{Q}^R_{i+1/2} = \mathbf{P}_{i+1}(x_{i+1/2})$. A Riemann problem with initial data composed of $\mathbf{Q}^L_{i+1/2}$ and $\mathbf{Q}^R_{i+1/2}$ is then posed. Godunov [14] suggested that the self-similar solution of the local Riemann problem with initial condition consisting of the constant states $\mathbf{Q}^L_{i+1/2}$ and $\mathbf{Q}^R_{i+1/2}$ be used to compute the numerical flux, setting in this way the basis for upwind methods. In this case there is no reconstruction and $\mathbf{Q}^L_{i+1/2} = \mathbf{Q}^n_i$, $\mathbf{Q}^R_{i+1/2} = \mathbf{Q}^n_{i+1}$. The original first-order upwind Godunov scheme uses the exact solution of this problem. Later, many researches, including Godunov himself [14], proposed to use the approximate solutions in the construction of upwind fluxes. Examples of such fluxes include the Rusanov flux [36], Osher-Solomon flux [13, 32], Roe flux [34], HLL flux of Harten *et al.* [21] and HLLC flux of Toro *et al.* [47, 55, 56]. A distinguishing feature of upwind fluxes is that they explicitly utilise information on wave propagation contained in the governing equations. Centred fluxes, on the other hand, do not explicitly use wave propagation information. This makes them very simple, efficient and applicable to problems where the Riemann problem solution is not known or is too costly to be used. The Lax-Friedrichs flux [27] is probably the most well-known first-order monotone centred flux. Other examples are the Godunov first-order centred flux [51] (not monotone) and the FORCE flux of Toro [48, 51, 49]. However, there

is a price to be paid for the simplicity of centred fluxes: in general, the more sophisticated upwind fluxes give results that are far superior to those of centred fluxes, especially for linear waves and large output times, provided *complete* Riemann solvers are used.

Usually, only lower order (first order) monotone fluxes are used as the building block for the construction of higher order schemes. In this paper we propose to use second order TVD fluxes as the building block in high order methods and apply the principle to the finite-volume ENO, WENO and MPWENO schemes. We call the new improved schemes the ENO-TVD, WENO-TVD and MPWENO-TVD schemes respectively. There appear to be two candidate fluxes that can be readily used as the building block for very high order schemes. These are the fluxes of the **F**lux **Li**miter **C**entred scheme (FLIC) of Toro and Billett [50] and that of the **W**eighted **A**verage **F**lux (WAF) scheme of Toro [52, 53, 51]. Both fluxes achieve second order of accuracy in space and time *without performing data reconstruction*, and this appears to be the key issue. The WAF flux is an upwind flux and can be used with any exact or approximate Riemann solver available. We recommend using *complete* Riemann solvers that include all waves in the Riemann problem solution. The FLIC flux is centred and requires no (explicit) wave propagation information.

Numerical results suggest that the new methods proposed here improve upon the original ENO, WENO and MPWENO methods in terms of better convergence, higher overall accuracy and better resolution of discontinuities in linearly degenerate fields, such as contact discontinuities. This is especially evident for long time evolution problems and coarse meshes.

The idea of using a second order TVD flux as the building block can in principle be applied to other very high order methods, such as RKDG and ADER methods. See [58] for application to the ADER approach in one space dimension.

The paper is organised as follows. In Section 2 we briefly review the framework for constructing finite-volume ENO, WENO and MPWENO schemes. In Section 3 we review the fluxes to be used as the building block in the methods. Numerical results are presented in Section 4 and conclusions are drawn in Section 5.

2. THE NUMERICAL SCHEME

In this section we review the construction of high order finite-volume schemes for hyper-

bolic systems in conservation form

$$\partial_t \mathbf{Q} + \partial_x \mathbf{F}(\mathbf{Q}) = \mathbf{0}, \tag{1}$$

along with initial and boundary conditions. Here $\mathbf{Q}(x,t)$ is the vector of unknown conservative variables and $\mathbf{F}(\mathbf{Q})$ is the physical flux vector.

There are essentially two ways to discretise (1). The first way is to develop *fully discrete* (one-step) schemes. Consider a control volume in $x-t$ space $[x_{i-1/2}, x_{i+1/2}] \times [t^n, t^{n+1}]$, of dimensions $\Delta x = x_{i+1/2} - x_{i-1/2}$, $\Delta t = t^{n+1} - t^n$. Integrating (1) with respect to x and t over the volume we obtain

$$\int_{x_{i-1/2}}^{x_{i+1/2}} \left[\mathbf{Q}(x,t^{n+1}) - \mathbf{Q}(x,t^n)\right] dx + \int_{t^n}^{t^{n+1}} \left[\mathbf{F}(\mathbf{Q}(x_{i+1/2},t)) - \mathbf{F}(\mathbf{Q}(x_{i-1/2},t))\right] dt = \mathbf{0}. \tag{2}$$

This results in the following numerical scheme

$$\mathbf{Q}_i^{n+1} = \mathbf{Q}_i^n - \frac{\Delta t}{\Delta x}\left[\mathbf{F}_{i+1/2} - \mathbf{F}_{i-1/2}\right], \tag{3}$$

where $\mathbf{Q}_i^n$ is the space average of the solution in the cell $[x_{i-1/2}, x_{i+1/2}]$ at time t^n and the numerical flux $\mathbf{F}_{i+1/2}$ is the time average of the physical flux at the cell interface $x_{i+1/2}$:

$$\mathbf{Q}_i^n = \frac{1}{\Delta x}\int_{x_{i-1/2}}^{x_{i+1/2}} \mathbf{Q}(x,t^n)\, dx, \quad \mathbf{F}_{i+1/2} = \frac{1}{\Delta t}\int_{t^n}^{t^{n+1}} \mathbf{F}(\mathbf{Q}(x_{i+1/2},t))\, dt. \tag{4}$$

Examples of very high order fully discrete schemes include ENO schemes [20] and ADER schemes [54, 44, 57, 45, 37, 58, 43].

Another way to discretise (1) is to keep the time variable t continuous and consider *semi-discrete* schemes. Integrating (1) with respect to x only we obtain the following system of ordinary differential equations (ODE):

$$\frac{d}{dt}\mathbf{Q}_i(t) = -\frac{1}{\Delta x}\left(\mathbf{F}_{i+1/2} - \mathbf{F}_{i-1/2}\right) = \mathbf{L}_i(\mathbf{Q}), \tag{5}$$

where $\mathbf{Q}_i(t)$ is the space average of the solution in the cell $[x_{i-1/2}, x_{i+1/2}]$ at time t and $\mathbf{F}_{i+1/2} = \mathbf{F}(\mathbf{Q}(x_{i+1/2},t))$ is the numerical flux at $x = x_{i+1/2}$ and time t:

$$\mathbf{Q}_i(t) = \frac{1}{\Delta x}\int_{x_{i-1/2}}^{x_{i+1/2}} \mathbf{Q}(x,t)\, dx, \quad \mathbf{F}_{i+1/2} = \mathbf{F}(\mathbf{Q}(x_{i+1/2},t)). \tag{6}$$

Note that the numerical flux of the semi-discrete scheme (6) is different from that of the fully discrete scheme (3). In current ENO and WENO schemes the numerical solution of (5)

is advanced in time by means of a TVD Runge-Kutta method [39]. Usually the following third order TVD Runge-Kutta method is used [40, 18, 1] (here we dropped the index i)

$$\begin{aligned}
\mathbf{Q}^{(n+1/3)} &= \mathbf{Q}^n + \Delta t\, \mathbf{L}(\mathbf{Q}^n), \\
\mathbf{Q}^{(n+2/3)} &= \frac{3}{4}\mathbf{Q}^n + \frac{1}{4}\mathbf{Q}^{(n+1/3)} + \frac{1}{4}\Delta t\, \mathbf{L}(\mathbf{Q}^{(n+1/3)}), \\
\mathbf{Q}^{n+1} &= \frac{1}{3}\mathbf{Q}^n + \frac{2}{3}\mathbf{Q}^{(n+2/3)} + \frac{2}{3}\Delta t\, \mathbf{L}(\mathbf{Q}^{(n+2/3)}).
\end{aligned} \tag{7}$$

Semi-discrete finite-volume ENO and WENO schemes are reported in [8, 30, 22, 38]. We note that one can also consider semi-discrere *finite-difference* schemes [40, 18, 41, 1], which work with point-wise values rather than cell averages. Here we consider finite-volume schemes only. We remark that using only the first (Euler) step of the Runge-Kutta method (7) and piece-wise constant reconstruction one obtaines a fully discrete first or second order scheme.

The numerical flux at the cell boundary $x_{i+1/2}$ is defined as a monotone function of left and right extrapolated values $\mathbf{Q}^L_{i+1/2}$, $\mathbf{Q}^R_{i+1/2}$:

$$\mathbf{F}_{i+1/2} = \mathbf{F}(\mathbf{Q}_{i+1/2}(t)) = \mathbf{F}_{i+1/2}(\mathbf{Q}^L_{i+1/2}, \mathbf{Q}^R_{i+1/2}). \tag{8}$$

These extrapolated values are obtained from cell averages by means of a high order polynomial reconstruction such as ENO [20, 40], WENO [30, 18], MP [41] or MPWENO reconstructions [1]. For example, for a scalar function $q(x)$ the fifth order WENO reconstruction defines the left extrapolated value $q^L_{i+1/2}$ as

$$q^L_{i+1/2} = \omega_0 v_0 + \omega_1 v_1 + \omega_2 v_2, \tag{9}$$

where v_k is the extrapolated value obtained from cell averages in the k^{th} stencil $S_k = (i-k, i-k+1, i-k+2)$

$$\begin{aligned}
v_0 &= \frac{1}{6}(-q_{i+2} + 5q_{i+1} + 2q_i), \\
v_1 &= \frac{1}{6}(-q_{i-1} + 5q_i + 2q_{i+1}), \\
v_2 &= \frac{1}{6}(2q_{i-2} - 7q_{i-1} + 11q_i),
\end{aligned} \tag{10}$$

and ω_k are nonlinear WENO weights given by

$$\omega_0 = \frac{\alpha_0}{\alpha_0+\alpha_1+\alpha_2}, \quad \omega_1 = \frac{\alpha_1}{\alpha_0+\alpha_1+\alpha_2}, \quad \omega_2 = \frac{\alpha_2}{\alpha_0+\alpha_1+\alpha_2},$$
$$\alpha_0 = \frac{3}{10(10^{-6}+IS_0)^2}, \quad \alpha_1 = \frac{3}{5(10^{-6}+IS_1)^2}, \quad \alpha_2 = \frac{1}{10(10^{-6}+IS_2)^2}.$$

The smoothness indicators IS_k are [18]

$$\begin{aligned} IS_0 &= \frac{13}{12}(q_i - 2q_{i+1} + q_{i+2})^2 + \frac{1}{4}(3q_i - 4q_{i+1} + q_{i+2})^2, \\ IS_1 &= \frac{13}{12}(q_{i-1} - 2q_i + q_{i+1})^2 + \frac{1}{4}(q_{i-1} - q_{i+1})^2, \\ IS_2 &= \frac{13}{12}(q_{i-2} - 2q_{i-1} + q_i)^2 + \frac{1}{4}(q_{i-2} - 4q_{i-1} + q_i)^2. \end{aligned}$$

The right value $q^R_{i+1/2}$ is obtained by symmetry. It can be shown that if $q(x)$ is smooth in the k^{th} stencil then the corresponding weight ω_k is $O(1)$ and approaches the optimal, so-called *linear*, weight. Otherwise $\omega_k = O(\Delta x^4)$ so that the (oscillatory) values from stencils containing discontinuities are assigned nearly zero weights [30, 18]. For systems the reconstruction is carried out in characteristic variables rather than conservative variables and (9) is applied to each characteristic field [20, 30, 18]. It can shown that the use of conservative variables (in a component-wise manner) in the reconstruction results in oscillations even for simple test problems [20, 33].

The description of the scheme is complete when a proper non-oscillatory flux (8) is chosen. In the next section we review possible centred and upwind fluxes which can be used.

3. FLUXES

In this section we review different non-oscillatory fluxes that can be used as the building block in the semi-discrete ENO/WENO with TVD Runge-Kutta time stepping. We first briefly review some conventional monotone first order centred and upwind fluxes which are commonly used in the framework of the finite-volume WENO schemes. Then we review fluxes associated with fully-discrete second-order TVD schems, which will then be used as the building block for the high-order ENO/WENO schemes.

3.1. Centred fluxes for first-order and second-order TVD schemes

Centred (or symmetric) fluxes contain no explicit wave propagation information (no upwinding). This makes them simple, efficient and applicable to very complex equations but also very diffusive as compared to upwind fluxes. In particular, waves associated with linearly degenerate fields, such as contact waves, shear waves and vortices, are poorly resolved.

It should be noted that although centred fluxes formally do not require any explicit information about wave propagation this information is still needed for enforcing a stability

condition for explicit methods. For explicit ENO, WENO and MPWENO schemes the *linear* stability condition reads

$$CFL \leq 1\,. \tag{11}$$

Here CFL denotes the maximum Courant number over all cells at a given time step:

$$CFL = \max_i \left(S_i^n \frac{\Delta t}{\Delta x} \right), \tag{12}$$

where S_i^n is the maximum propagation speed in the cell $[x_{i-1/2}, x_{i+1/2}]$ at time level n. We take it to be a bound of the eigenvalues of the Jacobian matrix $\mathbf{A}(\mathbf{Q}_i^n)$

$$S_i^n = |u_i^n| + a_i^n, \quad a_i^n = \sqrt{\frac{\gamma p_i^n}{\rho_i^n}}.$$

Probably the most well-known centred monotone flux is the Lax-Friedrichs flux [27] given by

$$\begin{aligned} \mathbf{F}^{LF}_{i+1/2}(\mathbf{Q}^L_{i+1/2}, \mathbf{Q}^R_{i+1/2}) &= \frac{1}{2}(\mathbf{F}^L_{i+1/2} + \mathbf{F}^R_{i+1/2}) - \frac{1}{2}\frac{\Delta x}{\Delta t}(\mathbf{Q}^R_{i+1/2} - \mathbf{Q}^L_{i+1/2}), \\ \mathbf{F}^L_{i+1/2} = \mathbf{F}(\mathbf{Q}^L_{i+1/2}), &\quad \mathbf{F}^R_{i+1/2} = \mathbf{F}(\mathbf{Q}^R_{i+1/2}). \end{aligned} \tag{13}$$

The Lax-Friedrichs flux is commonly used in the design of some (but not all) high order centred methods [31, 29]. In the limiting case of piece-wise constant data $\mathbf{Q}^L_{i+1/2} = \mathbf{Q}^n_i$, $\mathbf{Q}^R_{i+1/2} = \mathbf{Q}^n_{i+1}$ this flux leads to a monotone first-order accurate fully discrete scheme.

A flux, associated with a second order scheme is the two-step Lax-Wendroff flux:

$$\begin{aligned} \mathbf{F}^{LW}_{i+1/2}(\mathbf{Q}^L_{i+1/2}, \mathbf{Q}^R_{i+1/2}) &= \mathbf{F}(\mathbf{Q}^{LW}_{i+1/2}), \\ \mathbf{Q}^{LW}_{i+1/2} = \frac{1}{2}(\mathbf{Q}^L_{i+1/2} + \mathbf{Q}^R_{i+1/2}) &- \frac{1}{2}\frac{\Delta t}{\Delta x}(\mathbf{F}^R_{i+1/2} - \mathbf{F}^L_{i+1/2}). \end{aligned} \tag{14}$$

In the limiting case of piece-wise constant data the intermediate state $\mathbf{Q}^{LW}_{i+1/2}$ is obtained by integrating (1) over the control volume $[x_i, x_{i+1}] \times [t^n, t^n + \Delta t/2]$ and using the integral form of the conservation law. The result is

$$\mathbf{F}^{LW}_{i+1/2}(\mathbf{Q}^L_{i+1/2}, \mathbf{Q}^R_{i+1/2}) = \mathbf{F}(\mathbf{Q}^{LW}_{i+1/2}), \quad \mathbf{Q}^{LW}_{i+1/2} = \frac{1}{2}(\mathbf{Q}^n_i + \mathbf{Q}^n_{i+1}) - \frac{1}{2}\frac{\Delta t}{\Delta x}(\mathbf{F}^n_{i+1} - \mathbf{F}^n_i). \tag{15}$$

Expression (14) is a generalisation of (15) to higher order reconstructions. When used in the fully discrete scheme given by (3) flux (15) leads to a linear (oscillatory) second-order accurate method in space and time.

The flux of the First-Order Centred Scheme (FORCE) [48, 51, 49] is derived as the deterministic version of the staggered-grid Random Choice Method:

$$\mathbf{F}^{FORCE}_{i+1/2}(\mathbf{Q}^L_{i+1/2}, \mathbf{Q}^R_{i+1/2}) = \frac{1}{4}\left(\mathbf{F}^L_{i+1/2} + 2\mathbf{F}(\mathbf{Q}^{LW}_{i+1/2}) + \mathbf{F}^R_{i+1/2} - \frac{\Delta x}{\Delta t}(\mathbf{Q}^R_{i+1/2} - \mathbf{Q}^L_{i+1/2}) \right), \tag{16}$$

where $\mathbf{Q}^{LW}_{i+1/2}$ is given in (14). It turns out that the above flux is an arithmetic mean of the Lax-Friedrichs and Law-Wendroff fluxes. When used in the fully discrete scheme given by (3) in the limiting case of piece-wise constant data this flux leads to a monotone first-order accurate method. It can be shown [48, 51, 49] that the numerical viscosity of the FORCE flux is smaller than that of the Lax-Friedrichs flux.

Now the idea is to substitute the use of the first order centred flux by some high order but non-oscillatory flux such as the flux of a Total Variation Diminishing (TVD) method. Most of the modern TVD fluxes achieve non-oscillatory behaviour by applying a certain monotonicity constraint on the boundary extrapolated values obtained from the reconstruction procedure. Thus, they cannot be used with the WENO schemes because the application of such a constraint to boundary extrapolated values $\mathbf{Q}^{L}_{i+1/2}$, $\mathbf{Q}^{R}_{i+1/2}$ would conflict with the sought high order accuracy of the scheme. To our knowledge the only centred second order non-oscillatory flux which does not need any constrains on $\mathbf{Q}^{L}_{i+1/2}$, $\mathbf{Q}^{R}_{i+1/2}$ is the flux of the Flux Limiter Centred (FLIC) scheme [50, 51]. This flux achieves second order of accuracy in space and time without performing data reconstruction. Thus, it can be used directly with boundary extrapolated values. In the limiting case of the piece-wise constant data the FLIC flux leads to a second-order centred fully discrete scheme.

The FLIC flux is a flux-limited version of the Law-Wendroff scheme using the FORCE flux as the lower-order monotone flux:

$$\mathbf{F}^{FLIC}_{i+1/2} = \mathbf{F}^{FORCE}_{i+1/2} + \varphi_{i+1/2}(\mathbf{F}^{LW}_{i+1/2} - \mathbf{F}^{FORCE}_{i+1/2}), \tag{17}$$

where $\varphi_{i+1/2}$ is a flux limiter. There are several possible choices of the flux limiter $\varphi_{i+1/2}$ [50, 51]. Here we use the limiter which is *analogous*, but *not equivalent* to the compressive SUPERBEE limiter of Roe [35] and is given by [50, 51]:

$$\varphi(r) = \begin{cases} 0, & r \leq 0 \\ 2r, & 0 \leq r \leq \frac{1}{2} \\ 1, & \frac{1}{2} \leq r \leq 1 \\ \min\left(2, \varphi_g + (1-\varphi_g)r\right), & r > 1 \end{cases} \tag{18}$$

where $r = r_{i+1/2}$ is the flow parameter and φ_g is given by

$$\varphi_g = (1 - CFL)/(1 + CFL). \tag{19}$$

Here CFL is the Courant number used to choose the time step, see (12). For the Euler equations we recommend the following procedure to choose the flow parameter. First we compute

$$r^L_{i+1/2} = \frac{\Delta E_{i-1/2}}{\Delta E_{i+1/2}}, \quad r^R_{i+1/2} = \frac{\Delta E_{i+3/2}}{\Delta E_{i+1/2}}, \tag{20}$$

where E is total energy and

$$\Delta E_{i+1/2} = E^R_{i+1/2} - E^L_{i+1/2}.$$

Recall that $E^R_{i+1/2}$ and $E^L_{i+1/2}$ are obtained from the reconstruction step. Then we compute the single flux limiter

$$\varphi_{i+1/2} = \min\left(\varphi(r^L_{i+1/2}), \varphi(r^R_{i+1/2})\right)$$

and apply it to all components of the flux in (17).

3.2. **Upwind fluxes for first-order and second-order TVD schemes**

Upwind fluxes utilise information on local wave propagation explicitly. Godunov [14] first introduced the idea of using the self-similar solution $\mathbf{Q}_*(x/t)$ of the local Riemann problem with inital conditions $(\mathbf{Q}^L_{i+1/2}, \mathbf{Q}^R_{i+1/2})$ to compute the upwind numerical flux. The use of the Riemann problem incorporates the physics of wave propagation into the numerical method and leads to more accurate results as compared to centred fluxes. The original Godunov scheme uses the exact Riemann solver and the flux is given as

$$\mathbf{F}^{GOD}_{i+1/2}(\mathbf{Q}^L_{i+1/2}, \mathbf{Q}^R_{i+1/2}) = \mathbf{F}(\mathbf{Q}_*(0)).$$

When used in scheme (3) this flux leads to a first order monotone upwind scheme.

For our upwind methods we specialise the presentation of the schemes as applied to the one-dimensional compressible Euler equations for a gamma-law gas

$$\left.\begin{aligned} \partial_t \mathbf{Q} + \partial_x \mathbf{F}(\mathbf{Q}) &= \mathbf{0} \\ \mathbf{Q} &= (\rho, m, E)^T \\ \mathbf{F}(\mathbf{Q}) &= \mathbf{Q}u + (0, p, pu)^T \\ p &= (\gamma - 1)(E - \tfrac{1}{2}\rho u^2) \end{aligned}\right\} \tag{21}$$

where ρ, u, p and E are density, velocity, pressure and total energy, respectively; $m = \rho u$ is momentum and γ is the ratio of specific heats.

Although exact Riemann solvers for gamma-law gases are quite fast now [51], they become costly and complicated for general equations of state as the calculation of the exact solution will involve a double iterative procedure. Later, many researches, including Godunov himself [14], proposed to use approximate solutions in the construction of upwind fluxes [36, 13, 32, 34, 21, 47, 55, 56]. When used in (3) these fluxes give the first order upwind Godunov scheme with an *approximate* Riemann solver.

An upwind flux which is particularly popular due to its simplicity is the Rusanov first order upwind flux [36]. It has been widely used recently in high order upwind WENO methods [30, 64, 22, 38], RKDG methods [9, 10, 11, 64] and even *centred* staggered WENO methods [33] (under the name of the Lax-Friedrichs flux). Assuming that an estimate S^+ for the maximum signal speeds for waves emerging from the Riemann problem solution with data $\mathbf{Q}^L_{i+1/2}$ and $\mathbf{Q}^R_{i+1/2}$ is known, the Rusanov flux is defined as

$$\mathbf{F}^{RUS}_{i+1/2} = \frac{1}{2}(\mathbf{F}^L_{i+1/2} + \mathbf{F}^R_{i+1/2}) - \frac{1}{2} S^+_{i+1/2}(\mathbf{Q}^R_{i+1/2} - \mathbf{Q}^L_{i+1/2}). \tag{22}$$

We note that explicit schemes with the stability condition (11) require that

$$S^+_{i+1/2} \leq \frac{\Delta x}{\Delta t}.$$

In the limiting case $S^+_{i+1/2} = \Delta x/\Delta t$ the upwind Rusanov flux (22) reduces to the centred Lax-Friedrichs flux (13).

Another well-known and popular upwind flux, the HLL flux [21], assumes a two-wave structure of the Riemann problem solution and disregards all other waves, such as waves associated with linearly degenerate fields. For the Euler equations these are the contact and shear waves. As a result, the resolution of contact discontinuities is very poor and similar to that of centred fluxes. The same applies to the Rusanov flux. Therefore, it is recommended to use the upwind fluxes with all waves in the Riemann problem solution included. Here we use the HLLC flux [47, 55, 56] which is an improved variant of the HLL flux [21] in that it contains the middle (contact) wave in the Riemann problem solution. We remark that the HLLC flux does not use linearisation of the equations and works well for low-density problems, performs well at sonic points, no entropy fix is needed. See [62, 63] for applications to Space-Time Discontinuous Galerkin Finite Element Methods, [17] for the MHD equations and [3] for implicit methods for compressible viscous and turbulent flows.

An updated version of HLLC for the 3D Euler equations is found in [51]. Assuming a three-wave structure with speed estimates given by $S^L_{i+1/2}$, $S^*_{i+1/2}$ and $S^R_{i+1/2}$ the HLLC flux

is given by

$$\mathbf{F}^{HLLC}_{i+1/2} = \begin{cases} \mathbf{F}^{L}_{i+1/2}, & \text{if} \quad 0 \le S^{L}_{i+1/2}\,, \\ \mathbf{F}^{*L}_{i+1/2} = \mathbf{F}^{L}_{i+1/2} + S^{L}_{i+1/2}(\mathbf{Q}^{*L}_{i+1/2} - \mathbf{Q}^{L}_{i+1/2})\,, & \text{if} \quad S^{L}_{i+1/2} \le 0 \le S^{*}_{i+1/2}\,, \\ \mathbf{F}^{*R}_{i+1/2} = \mathbf{F}^{R}_{i+1/2} + S^{R}_{i+1/2}(\mathbf{Q}^{*R}_{i+1/2} - \mathbf{Q}^{R}_{i+1/2})\,, & \text{if} \quad S^{*}_{i+1/2} \le 0 \le S^{R}_{i+1/2}\,, \\ \mathbf{F}^{R}_{i+1/2}, & \text{if} \quad 0 \ge S^{R}_{i+1/2}\,, \end{cases} \tag{23}$$

where

$$\mathbf{Q}^{*K}_{i+1/2} = \rho^{K}_{i+1/2}\left(\frac{S^{K}_{i+1/2} - u^{K}_{i+1/2}}{S^{K}_{i+1/2} - S^{*}_{i+1/2}}\right)\begin{bmatrix} 1 \\ S^{*}_{i+1/2} \\ v^{K}_{i+1/2} \\ w^{K}_{i+1/2} \\ \frac{E^{K}_{i+1/2}}{\rho^{K}_{i+1/2}}(S^{*}_{i+1/2} - u^{K}_{i+1/2})[S^{*}_{i+1/2} + \frac{p^{K}_{i+1/2}}{\rho^{K}_{i+1/2}(S^{K}_{i+1/2} - u^{K}_{i+1/2})}] \end{bmatrix}$$

for $K = L$ and $K = R$.

The wave speeds $S^{L}_{i+1/2}$, $S^{*}_{i+1/2}$ and $S^{R}_{i+1/2}$ must be estimated. We use the pressure-velocity estimates of Sect. 10.5.2 of [51]. For the Rusanov flux one can then take

$$S^{+} = \max\left(|S^{L}_{i+1/2}|, |S^{R}_{i+1/2}|\right).$$

Another way of estimating wave speeds can be found in [2].

Finally, we propose to use a second order upwind TVD flux as the building block in the high order ENO/WENO/MPWNO schemes. It appears as if the only upwind flux which does not impose any constrains on the boundary extrapolated values is the flux of the Weighted Average Flux (WAF) method, a second order TVD method.

The WAF method [52, 53, 51] defines an intercell flux as

$$\mathbf{F}^{WAF}_{i+1/2} = \frac{1}{t_2 - t_1}\frac{1}{x_2 - x_1}\int_{t_1}^{t_2}\int_{x_1}^{x_2} \mathbf{F}(\mathbf{Q}^{*}(x,t))\,dx\,dt\,. \tag{24}$$

A special case, and the one we use here, is the formula

$$\mathbf{F}^{WAF}_{i+1/2} = \frac{1}{\Delta x}\int_{-\Delta x/2}^{\Delta x/2} \mathbf{F}(\mathbf{Q}_{i+1/2}(x, t^n + \Delta t/2))\,dx. \tag{25}$$

Assuming further that $\mathbf{Q}_{i+1/2}$ is the solution of the conventional piece-wise constant Riemann problem with initial data $\mathbf{Q}^{L}_{i+1/2}$ and $\mathbf{Q}^{R}_{i+1/2}$ we may write

$$\mathbf{F}^{WAF}_{i+1/2} = \frac{1}{2}(\mathbf{F}^{L}_{i+1/2} + \mathbf{F}^{R}_{i+1/2}) - \frac{1}{2}\sum_{k=1}^{N} c_k \Delta\mathbf{F}^{(k)}_{i+1/2}, \tag{26}$$

where $c_k = \frac{S_k \Delta t}{\Delta x}$ is the Courant number associated with wave k of speed S_k in the solution of the Riemann problem. Flux (26) gives a linear (oscillatory) second order accurate scheme. A non-oscillatory, TVD, version is given by

$$\mathbf{F}^{WAF}_{i+1/2} = \frac{1}{2}(\mathbf{F}^{L}_{i+1/2} + \mathbf{F}^{R}_{i+1/2}) - \frac{1}{2}\sum_{k=1}^{N} \mathrm{sign}(c_k) A_k \Delta \mathbf{F}^{(k)}_{i+1/2}, \tag{27}$$

where A_k is a WAF flux limiter related to a conventional flux limiter B_k [42] via

$$A_k = 1 - (1 - |c_k|)B_k. \tag{28}$$

Here we use the WAF limiter that is *equivalent* to the compressive SUPERBEE limiter of Roe [35] and is given by (we omit index k) [51]

$$\varphi(r) = \begin{cases} 1, & r \le 0, \\ 1 - 2(1 - |c|)r, & 0 \le r \le \frac{1}{2}, \\ |c|, & \frac{1}{2} \le r \le 1, \\ 1 - 2(1 - |c|)r, & 1 \le r \le 2, \\ 2|c| - 1, & r > 2. \end{cases} \tag{29}$$

The flux limiter depends on a flow parameter $r^{(k)}$ which refers to wave k in the solution of the Riemann problem and is the ratio

$$r = \begin{cases} \dfrac{\Delta q^{(k)}_{i-1/2}}{\Delta q^{(k)}_{i+1/2}}, & \text{if} \quad c_k > 0, \\ \dfrac{\Delta q^{(k)}_{i+3/2}}{\Delta q^{(k)}_{i+1/2}}, & \text{if} \quad c_k < 0, \end{cases} \tag{30}$$

where $q^{(k)}$ is a suitable variable depending on the problem being solved. This variable must change across each wave family in the solution of the Riemann problem. $\Delta q^{(k)}_{l+1/2}$ denotes the jump in q across wave k in the self-similar solution $\mathbf{Q}_{l+1/2}(\xi/\tau)$ in the Riemann problem with data $(\mathbf{Q}^{L}_{l+1/2}, \mathbf{Q}^{R}_{l+1/2})$ at cell interface $x_{l+1/2}$. For the Euler equations the choice $q = \rho$ (density) usually gives very satisfactory results.

The WAF method can be used with any Riemann solver available. It is recommended to use *complete* Riemann solvers, that is those including all waves in their structure. In this paper we utilise the HLLC Riemann solver (23).

3.3. **TVD fluxes and TVD Runge-Kutta schemes**

In this paper we utilise fluxes associated with fully discrete second-order TVD (centred and upwind) methods as the building block for constructing high-order WENO semi-discrete schemes with Runge-Kutta time stepping. Shu [39] has developed TVD Runge-Kutta schemes, such as the third-order scheme (7), using a scheme of the form

$$\hat{\mathbf{Q}} = \bar{\mathbf{Q}} + \Delta t \mathbf{L}(\bar{\mathbf{Q}}), \tag{31}$$

in which the right-hand side is a forward-Euler type stepping, assumed to be TVD (Total Variation Diminishing), that is

$$TV(\hat{\mathbf{Q}}) \leq TV(\bar{\mathbf{Q}}). \tag{32}$$

Our fully discrete second-order TVD schemes discussed earlier can also be expressed in the form (31), with

$$\mathbf{L}(\bar{\mathbf{Q}}) = -\frac{1}{\Delta x}\left[\mathbf{F}^{TVD}_{i+\frac{1}{2}} - \mathbf{F}^{TVD}_{i-\frac{1}{2}}\right], \tag{33}$$

where $\mathbf{F}^{TVD}_{i+\frac{1}{2}}$ is either the centred FLIC flux (17) or WAF flux (27).

It is easy to verify that given a TVD Runge-Kutta scheme based on a forward Euler type stepping of the form (31), (33) the corresponding Runge-Kutta scheme remains TVD if the operator $\mathbf{L}$ is given by (33). For example, for the third-order scheme (7) we have

$$TV(\mathbf{Q}^{n+1}) \leq TV(\mathbf{Q}^n), \tag{34}$$

which is easily verified, namely

$$\begin{aligned} TV(\mathbf{Q}^{n+1}) &= TV\left(\frac{1}{3}\mathbf{Q}^n + \frac{2}{3}\left[\mathbf{Q}^{(n+2/3)} + \Delta t \mathbf{L}(\bar{\mathbf{Q}}^{(n+2/3)})\right]\right) \\ &\leq \frac{1}{3}TV(\mathbf{Q}^n) + \frac{2}{3}TV(\mathbf{Q}^{(n+2/3)}) \\ &\quad \cdots \\ &\leq \frac{1}{3}TV(\mathbf{Q}^n) + \frac{1}{2}TV(\mathbf{Q}^n) + \frac{1}{6}TV(\mathbf{Q}^n) \\ &= TV(\mathbf{Q}^n). \end{aligned} \tag{35}$$

It is important to realise that in the case of no reconstruction (piece-wise constant representation of the solution inside a cell) the original WENO schemes with first order fluxes as the building block reduce to a first order monotone scheme whereas the WENO-TVD schemes presented here reduce to a *second order* TVD scheme.

To complete this section we address some implementation issues. When the solution contains strong shocks it may be beneficial to use characteristic projections in the evaluation of the WAF flux when the compressive SUPERBEE limiter is used; see [58] for implementation details. However, we find that for the WENO schemes this procedure is unnecessary. It is known that the use of compressive limiters in TVD schemes affects, in an adverse manner, smooth parts of the solution, the effect known as *squaring*. However, in the framework of higher order WENO schemes the squaring effect is smoothed out, retaining the extra benefits of a compressive limiter in resolving discontinuities, particularly contact discontinuities. This will be become apparent in the numerical results shown in the next section.

The computation of the ratio r in (20) and (30) requires special attention when the denominator D is small, $|D| \leq \varepsilon$, say, where ε is a small positive number. For TVD methods, experience shows that the robustness of the methods does not depend too crucially on the way this step is handled, while accuracy does. For the computations reported in this paper, the following procedure was applied:

$$r = \frac{\hat{N}}{\hat{D}}, \quad \hat{X} = \begin{cases} \varepsilon \,\mathrm{sign}(1, X), & if \quad |X| \leq \varepsilon, \\ X, & \text{otherwise}, \end{cases} \tag{36}$$

where we take $\varepsilon = 10^{-6}$. From (36) it can be easily seen that for nearly uniform flow $r \approx 1$, leading to second order accuracy, the correct behaviour of a TVD scheme. It seems to us as if the implementation of TVD criteria in the context of the construction of very high-order methods may require some further investigations.

4. NUMERICAL RESULTS

In this section we compare numerical results of the new schemes proposed here with those of the corresponding original schemes. The new schemes differ from the original schemes of [40, 18, 1] in that they use second order TVD fluxes whereas the original schemes employ only first order monotone fluxes. Here we choose Lax-Friedrichs (13) and HLLC fluxes (23) as the representatives of first-order monotone centred and upwind fluxes and the FLIC (17) and WAF (27) fluxes as the representatives of second-order centred and upwind TVD fluxes respectively. We consider spatially third order ENO, spatially fifth order WENO and spatially ninth order MPWENO schemes with these fluxes. For the time discretization we use, throughout, the third order TVD Runge-Kutta method (7) and therefore the formal

accuracy of these schemes is third. For brevity in the rest of the paper when referring to the accuracy of ENO, WENO and MPWENO schemes we mean the spatial accuracy. To save space we pay more attention to the fifth order WENO schemes with the reconstruction given by (9); these are original WENO-LF and WENO-HLLC schemes and new WENO-FLIC and WENO-WAF schemes. We also include the results of basic second order TVD schemes, namely the WAF and FLIC schemes.

There is a number of limiters which can be used with second order non-oscillatory TVD fluxes. In this paper for the WENO-TVD schemes (WENO-FLIC and WENO-WAF) we use the compressive limiters given by (18) and (29). For the basic TVD schemes (FLIC and WAF) we use smooth limiters, namely the van Leer limiter [61] for the WAF scheme and the analagous (*not equivalent*) limiter for the FLIC scheme [50, 51]. We do so because in our numerical experiments the compressive limiters give more accurate results than the smooth limiters when used in the WENO-TVD schemes but show undesirable *squaring* of the smooth parts of the solution when used with second order TVD schemes. This behaviour of TVD schemes associated with overcompressive limiters is well known.

An important issue is the choice of the Courant number, which defines the time step. The WENO schemes are linearly stable for Courant numbers up to unity [18]. However, for solutions with discontinuities smaller Courant numbers are usually used, typically in the range of 0.2-0.6. For larger Courant numbers, e.g. 0.9, the WENO schemes become oscillatory in some of our numerical experiments. The same observation applies to other schemes with Runge-Kutta time discretisation, e.g. finite-difference ENO [40] and MPWENO [1] schemes. It is argued [1] that this behavior of the WENO schemes is due to the combination of the lower order time discretisation and higher order spatial reconstruction. In this paper we use CFL=0.4 for the WENO schemes throughout, where CFL denotes the maximum Courant number for each time step, see (12). For the MPWENO schemes we use CFL=0.3, which is consistent with the requirement of the monotonicity constraint [41] used in this scheme. For all calculations made with the WAF and FLIC schemes we use CFL=0.95 throughout.

In the numerical experiments we use very large output times, corresponding to hundreds of thousand of time steps. We remark that there is no point in using expensive and complex very high order methods for short-time propagation problems since for such problems conventional TVD schemes often give acceptable results while being much faster and simpler. The sophistication of very high order methods can be justified only for very long time

propagation.

We also pay special attention to the accuracy of the methods on *coarse meshes* and for solutions containing delicate features such as contact discontinuities. Of course, all convergent methods will give the same results in the limit of zero cell size. The point is that a very high order method should outperform a conventional TVD method on all meshes, particularly on very coarse meshes.

4.1 Scalar linear advection

First we solve a test problem with a very smooth solution in order to see how the TVD fluxes with compressive limiters influence the convergence properties of the WENO-TVD schemes.

4.1.1. *Example 1: smooth solution*

We solve

$$\partial_t q + \partial_x q = 0, \tag{37}$$

with the initial condition

$$q(x,0) = \sin^4(\pi x) \tag{38}$$

defined on [-1,1] and periodic boundary conditions. We use output times $t = 1$ and $t = 1000$. Tables 1 and 2 show convergence rates and errors in different norms for cell averages of the solution for the TVD, WENO and WENO-TVD schemes.

We observe that for the output time $t = 1$ original WENO schemes and new WENO-TVD schemes converge with approximately forth order of accuracy. The use of the compressive SUPERBEE-type limiters in the WENO-TVD schemes degrades neither the convergence rate nor the size of the error. This result is very satisfactory as it shows that second order TVD fluxes with compressive limiters can be used in the higher order methods (higher than second order) without affecting the convergence properties. In fact, on coarse meshes we observe some gains in accuracy.

The situation is different for the second, much larger, output time $t = 1000$. The WAF, WENO-HLLC and WENO-TVD schemes are seen to converge much better than the centred FLIC and WENO-LF schemes. For the latter schemes the mesh refinements from 20 to 160 cells have virtually no effect on the size of the error. In fact, for these meshes the second

order (only first order in L_∞ norm) upwind TVD scheme WAF is more accurate than the third order (fifth order in space) WENO-LF scheme. This is surprising because for smooth solutions the higher order schemes, such as WENO schemes, are believed to produce much better results than conventional second order TVD schemes, no matter which flux is used as the building block in the scheme. Clearly, the use of the Lax-Friedrichs flux significantly affects the convergence of the WENO-LF scheme. Comparing the results of the WENO-TVD and original WENO schemes we observe that the use of TVD fluxes improves the accuracy and convergence properties of the schemes.

4.1.2. *Example 2: solution containing discontinuities*

Now we solve equation (37) for the following initial condition [18, 41, 1]

$$q(x,0) = \begin{cases} \exp\left(\ln 2\,(x+0.7)^2/0.0009\right), & -0.8 \le x \le -0.6, \\ 1, & -0.4 \le x \le -0.2, \\ 1-|10x-1|, & 0.0 \le x \le 0.2, \\ (1-100(x-0.5)^2)^{1/2}, & 0.4 \le x \le 0.6, \\ 0, & \text{otherwise}, \end{cases} \tag{39}$$

and periodic boundary conditions. This time the solution is a combination of a discontinuous square pulse and several continuous but narrow profiles. This is the type of problems for which WENO schemes have to be used with smaller CFL numbers than allowed by the linear stability analysis; e.g. CFL=0.2-0.4 are used in [18, 41, 1]. We compute the solution at the output times $t = 20$ (short time evolution) and $t = 2000$ (long time evolution). For the second output time the initial profile is propagated 1000 times over the spatial domain; when CFL number of unity is used, it corresponds to 2×10^5 time steps.

Table 3 shows convergence studies for cell averages of the solution *in the* L_1 *norm*; in this norm all schemes should converge with first order of accuracy. We observe that for the small output time $t = 20$ (10 periods) all schemes converge with first order of accuracy except the WENO-LF scheme, which suffers a loss of convergence rate as the mesh is refined. The situation is again very different when we consider the second, much larger output time $t = 2000$ (1000 periods). The WENO-LF scheme converges very poorly; the mesh refinement from 400 to 1600 cells has virtually no effect on the size of the error. All other schemes achieve

approximately first order of accuracy as the mesh is refined. We note that the WAF scheme outperforms the centred FLIC and WENO-LF schemes and the original upwind WENO-HLLC scheme. As expected, the WENO-TVD schemes are superior schemes to the original WENO schemes. In particular, the WENO-FLIC scheme outperforms other centred schemes (FLIC and WENO-LF). Namely, on the finest mesh of 1600 cells WENO-FLIC is more than 10 times more accurate than WENO-LF and around 5 times more accurate than the FLIC scheme. The WENO-WAF scheme produces the most accurate results of all methods; its error is more than 3 times smaller that that of the WENO-HLLC scheme and 2 times smaller than that of the WAF scheme. We also remark that overall, for the second output time, upwind methods perform much better than centred methods.

Figs. 1-6 depict graphical results of various methods for the output time $t = 2000$ on the mesh of 200 cells. In all figures the continuous line corresponds to the exact solution and symbols correspond to the numerical solution. We observe that the centred FLIC and WENO-LF schemes produce unacceptable results of virtually the same accuracy; namely the numerical solution does not contain any of the features present in the exact solution. The WAF scheme performs better but still the accuracy is very poor. A surprising observation is that the accuracy of the second order TVD scheme WAF is overall higher than that of the fifth order WENO-LF scheme. Other WENO schemes, namely the WENO-HLLC, WENO-FLIC and WENO-WAF schemes produce much more accurate results. In particular, the new centred WENO-FLIC scheme is significantly more accurate than the original WENO-LF scheme. Overall, for the given mesh the WENO-WAF is the most accurate scheme.

Figs. 7-12 depict graphical results of various methods for the output time $t = 2000$ on the finest mesh of 1600 cells. We see that on this mesh the WAF scheme outperforms the FLIC scheme and original WENO-LF and WENO-HLLC schemes, compare Figs. 10 with Figs. 7, 8 and 11. In particular, WAF provides better resolution of the discontinous square pulse. As before, the WENO-LF scheme is the least accurate scheme. As expected, the WENO-TVD schemes produce the most accurate results for all parts of the solution, including the square pulse. These observations are in good agreement with the convergence study of Table 3. We remark that there are some oscillations in the result of the WENO-FLIC scheme on the finest mesh; these may be related to the way the flow parameter r, given by (20), is computed. A similar effect was observed for the forth order ADER-WAF scheme in [58].

The numerical results for the linear advection equation with constant coefficient lead

us to believe that the TVD schemes, especially upwind schemes such as WAF, are not to be ruled out when compared with the very high order centred schemes, particularly with those using the Lax-Friedrichs flux as the building block. This is especially so for long time evolution problems. The simplicity and efficiency of the TVD schemes, as compared with the higher order WENO schemes, should also be taken into account. We believe that this statement applies not only to the WENO-LF scheme but also to other modern centred schemes with the Lax-Friedrichs flux, such as those presented in [31, 26]. However, we expect the centred WENO (CWENO) scheme of Qiu and Shu [33] to produce results similar to those of the WENO-HLLC scheme when applied to the linear advection equation with constant coefficient. This is because this CWENO scheme actually uses the *upwind* Rusanov flux which coincides with the upwind Godunov flux in the linear scalar case.

The new ENO-TVD and MPWENO-TVD schemes show similar improvements over the original ENO and MPWENO schemes. For the MPWENO schemes these improvements in general are smaller than for ENO and WENO schemes, as one would expect. We omit the results here.

4.2 The Euler equations of gas dynamics

We now assess the performance of different schemes for the one-dimensional Euler equations for a γ-law gas (21), with $\gamma = 1.4$ in all the results shown here.

4.2.1. *Example 1: Stationary contact discontinuity.*

Consider the following initial condition [51] defined on $[0, 1]$:

$$(\rho, u, p) = \begin{cases} (1.4, 0.0, 1.0), & x < \frac{1}{2}, \\ (1.0, 0.0, 1.0), & x > \frac{1}{2}, \end{cases} \tag{40}$$

which corresponds to an isolated stationary contact discontinuity. A mesh of 50 cells is used. On this mesh at $t = 0$ the discontinuity is positioned at the cell interface. We run the schemes until the steady state solution is reached.

Table 4 shows the errors of different schemes in the L_1 norm, the number of time steps needed to achieve the steady state solution and the number of cells across the contact discontinuity. Figs. 13 - 15 depict graphical results for the WENO-LF, MPWENO-LF and WENO-FLIC methods. We observe that the methods with *complete* upwind fluxes

resolve the isolated contact discontinuity exactly. This is expected since the HLLC Riemann solver used in these schemes recognises the middle (contact) wave in the Riemann problem solution. A surprising observation is that the schemes with the centred FLIC flux resolve the contact discontinuity exactly. This is due to our choice of total energy as the quantity for the flow parameter r in (20). Recall that total energy is continuous across the contact discontinuity. Therefore $r = 1$ and the FLIC flux reduces to the Lax-Wendroff flux. From the Rankine-Hugoniot conditions for the stationary discontinuity it follows that the physical flux is continuous across the stationary discontinuity. It is obvious that in this situation the Lax-Wendroff flux does not introduce any perturbations to the discontinuity. As a result, the contact discontinuity is not smeared by the FLIC flux. The schemes which use the Lax-Friedrichs flux as the building block (ENO-LF, WENO-LF and MPWENO-LF) smear the discontinuity as time evolves. The reason for this is that the vector of conservative variables is *not* continuous across the stationary contact discontinuity and at each time step the Lax-Friedrichs flux introduces a perturbation to the exact profile. This perturbation is proportional to the density jump across the discontinuity. However, the smearing becomes smaller as the spatial order of the scheme increases.

4.2.2. *Example 2: Shock/turbulence interaction problem.*

We compare the performance of different schemes on a problem with a rich smooth structure and a shock wave. We use the following test problem [58], which is a variation of the shock/turbulence problem proposed in [18, 1]. The initial condition defined on $[-5, 5]$ is

$$(\rho, u, p) = \begin{cases} (1.515695, 0.523346, 1.80500), & x < -4.5, \\ (1 + 0.1 \sin 20\pi x, 0.0, 1.), & x > -4.5, \end{cases} \tag{41}$$

which consists of a right-facing shock wave of Mach number 1.1 running into a high-frequency density perturbation. The flow contains physical oscillations which have to be resolved by the numerical method. We compute the solution at the output time $t = 5$, which is more than ten times larger than that of the standard shock/turbulence problem of [1]. Figs. 16-21 show results of the TVD, original WENO and new WENO-TVD schemes on a mesh of 2000 cells. In all figures the continuous line corresponds to the reference solution and symbols correspond to the numerical solution. The reference solution is obtained by applying the fifth order ADER5-WAF scheme [58] on a fine mesh of 5000 cells and is shown by the solid

line on all figures.

Figs. 16-18 depict graphical results for the centred FLIC, WENO-LF and WENO-FLIC schemes. We see that the FLIC and WENO-LF schemes produce very inaccurate results. In particular, the undisturbed region ahead of the shock wave is poorly resolved by the WENO-LF scheme. The WENO-FLIC scheme offers much better accuracy. The improvement over the WENO-LF is most remarkable since these centred schemes differ only in the flux used, namely the Lax-Friedrichs flux (first order) versus the FLIC flux (second order TVD).

Figs. 19-21 depict graphical results for the upwind WAF, WENO-HLLC and WENO-WAF schemes. We observe the clear improvements in accuracy as we move from the TVD WAF scheme to the WENO-HLLC scheme and to the WENO-WAF scheme. Note that the undisturbed region ahead of the shock wave is well resolved by all these upwind schemes. The WENO-WAF scheme produces the most accurate solution, which is very close to the reference solution.

Comparing the numerical results of the centred (Figs. 16-18) and upwind (Figs. 19-21) schemes we observe that the upwind schemes are clearly superior. On the given mesh the second order (only first order in the L_∞ norm) WAF scheme outperforms not only the FLIC scheme but also the fifth order WENO-LF scheme. We also note that the WAF scheme with the SUPERBEE limiter is even more accurate for this problem; the result is omitted here. The most accurate centred scheme, the WENO-FLIC scheme, only approaches the accuracy of the upwind WENO-HLLC scheme and is much less accurate than the most accurate upwind scheme, the WENO-WAF scheme.

Another way of interpreting the results of Fig. 18 and Fig. 20 is this: by using a centred TVD flux as a building block for very high order methods one *approaches* the accuracy of the corresponding method used with a first order monotone upwind flux based on a *complete* Riemann solver. The attaraction of the centred second-order TVD flux is that it is simpler and more general than a good upwind flux, such as the HLLC, for example. However, the differences in accuracy between the centred-based and upwind-based are still clearly visible. See also Figs. 23 and 24 for ENO schemes and Figs. 27 and 28 for MPWENO schemes.

It should be noted that when the mesh is sufficiently refined the WENO-LF scheme outperforms, *to the eye*, the TVD WAF scheme with the van Leer limiter. When the more compressive SUPERBEE limiter is used, the WAF scheme still compares well with the WENO-LF scheme.

Figs. 22-25 depict graphical results of the ENO and ENO-TVD schemes on the mesh of 2000 cells and Figs. 26-29 depict graphical results of the MPWENO and MPWENO-TVD schemes on the coarser mesh of 1000 cells. We again observe that the schemes with the Lax-Friedrichs flux are the most diffusive whereas the schemes with the WAF flux are the most accurate. Overall, the new schemes are superior to the original schemes. It is remarkable that for this test problem the influence of the choice of the flux is equally large for schemes with least accurate (3^{th} order ENO) and most accurate (9^{th} order MPWENO) reconstructions.

We note that the shock wave here is rather weak and cannot be used to test the robustness of the new schemes. However, we have run the new schemes for the suit of test problems proposed by Toro [51] and obtained good results; these are omitted here.

4.3 Computing times and efficiency of the schemes

All calculations have been run on a personal computer with Athlon-XP 1700+ processer (1.533 Ghz clock frequency). We use Compaq Visual Fortran Compiler 6.0 with full optimisation to generate the corresponding code. Table 5 shows computing times for all schemes on the mesh of 2000 cells and given CFL numbers. The timings for ENO schemes are similar to those of WENO schemes and thus omitted. We note that the efficiency of the schemes depends on the hardware, compilers, coding and other factors. Therefore, our results may be different from those of other researchers. As expected, the TVD schemes are the fastest schemes. The fastest WENO scheme, WENO-LF, is around ten times slower than the TVD schemes. We note that our timings agree well with those presented in [18], where Jiang and Shu show that a single step of the Runge-Kutta time method of the WENO scheme is 3-4 times more expensive than that of a *typical* TVD scheme with MUSCL reconstruction in characteristic variables and a two-step Runge-Kutta method. This translates into 4.5-6 times difference in speed when the same CFL number is used because the WENO schemes use a three-step TVD Runge-Kutta method (7) as compared to a two-step Runge-Kutta method used by a TVD scheme. Also, the WENO schemes need smaller CFL numbers, here we use CFL=0.4 for the WENO schemes and CFL=0.95 for the TVD WAF scheme. Furthermore, the FLIC and WAF methods should be faster than a *typical* TVD scheme used for comparison in [18] because i) they are one-step methods, thus only one flux evaluation is needed per time step per cell interface, as compared to two flux evaluations in

the scheme with the Runge-Kutta time stepping; ii) they do not need any characteristic projections/reconstruction. All these factors result in the difference in speed tabulated in Table 5.

The WENO-FLIC scheme is only around 10% slower than the WENO-LF scheme. Considering the improvements in accuracy over the WENO-LF scheme, this additional computational cost is not significant.

The WENO-WAF scheme is around 30% slower that the WENO-HLLC scheme. This is due to the use of the more expensive WAF flux instead of the first order HLLC flux in each step of the Runge-Kutta method. However, again this difference in speed is more than compensated by the improvement in accuracy.

For the given CFL numbers the MPWENO scheme is around 2.5 times slower than the corresponding WENO scheme when the same flux is used. This is due to the much more costly reconstruction procedure used. We note that the MPWENO-WAF scheme is only 10% slower than the MPWENO-HLLC scheme; therefore it is worth using the WAF flux with this scheme. Balsara and Shu [1] point out that the 9^{th} order WENO reconstruction alone is around three times more expensive than the fifth order WENO reconstruction. On top of that one has to add the computational cost of applying the monotonicity-preserving bounds developed in [41] and a smaller CFL number as compared to the WENO scheme. On the other hand, for the Euler equations , there are other steps in the method, such as flux evaluation and characteristic projections; therefore the difference in speed between the WENO and MPWENO schemes for the CFL numbers used is only around 2.5 times. For the numerical results presented this difference is more than compensated by the improvements in accuracy associated with the higher order reconstruction.

5. CONCLUSIONS

In this paper we have proposed to use a second order TVD flux, rather than a first order monotone flux, as the building block for constructing very-high order methods and have applied the idea to finite-volume ENO, WENO and MPWENO schemes. We call the new schemes the ENO-TVD, WENO-TVD and MPWENO-TVD schemes. As the building block we consider the centred FLIC flux and upwind WAF flux together with compressive SUPERBEE-type limiters. Both upwind and centred new schemes use the same reconstruction and time discretisation as do the original upwind finite-volume schemes.

The centred ENO-FLIC, WENO-FLIC and MPENO-FLIC schemes, proposed in the paper, do not use staggered meshes, which are common in other centred methods such as those in [31, 33]. Also, our centred scheme does not suffer from large numerical diffusion, typical of conventional centred schemes with the Lax-Friedrichs flux. In particular, the new schemes with the FLIC flux resolve stationary contact discontinuities *exactly*.

The numerical results of the proposed schemes for the linear advection equation with constant coefficient and for the Euler equations show remarkable improvements over the corresponding original schemes with first order monotone centred and upwind fluxes, especially for long time evolution problems containing both smooth and non-smooth features. In addition, our numerical results lead us to believe that the TVD schemes, both centred FLIC and upwind WAF, are not to be ruled out when compared with the very high order centred schemes using the Lax-Friedrichs flux as the building block. We show that the schemes with the Lax-Friedrichs flux are not suitable for long time evolution problems due to excesive numerical diffusion. The above-mentioned differences in accuracy between upwind and centred fluxes and between first order and second order fluxes exist for schemes of all spatial orders.

Future work will include extensions of the present results to multidimensional WENO schemes as well as to other high-order methods such as the Runge-Kutta Discontinuous Galerkin methods [9, 10, 11].

Acknowledgments. The paper was finalized during the stay of the first author at the Isaac Newton Institute for Mathematical Sciences, University of Cambridge and participation in the programme *Nonlinear Hyperbolic Waves in Phase Dynamics and Astrophysics.* The second author acknowledges the support provided by the Isaac Newton Institute for Mathematical Sciences, University of Cambridge, UK, as organizer of the six-month programme on *Nonlinear Hyperbolic Waves in Phase Dynamics and Astrophysics*, January to July 2003, and the associated EPSRC senior visiting fellowship, grant No GR N09276.

References

[1] Balsara D. S. and Shu C.W. (2000). Monotonicity preserving weighted essentially non-oscillatory schemes with increasingly high order of accuracy. *J. Comp. Phys.*, **160**, pp.

405-452.

[2] Batten P., Clarke N., Lambert C. and Causon D.M. (1997). On the choice of wave speeds for the HLLC Riemann solver. *SIAM J. Sci. Stat. Comput.*, **18**(6), pp. 1553-1570

[3] Batten P. , Leschziner M. A. and Goldberg U. C. (1997). Average-State Jacobians and Implicit Methods for Compressible Viscous and Turbulent Flows. *J. Comp. Phys.*,**137**, pp. 38-78.

[4] Ben-Artzi M. and Falcovitz J. (1984). A Second–Order Godunov–Type Scheme for Compressible Fluid Dynamics. *J. Comp. Phys.*, **55**, 1–32.

[5] Boris J.P. and Book D.L. (1973). Flux-Corrected Transport I. SHASTA, A Fluid Transport Algorithm That Works. *J. Comp. Phys.*, **11** (1).

[6] Book D.L., Boris J.P. and Hain K. (1975). Flux-Corrected Transport II: Generalizations of the Method. *J. Comp. Phys.*, **18** (3), pp. 248-283.

[7] Boris J.P. and Book D.L. (1976). Flux-Corrected Transport III: Minimal-Error FCT Algorithms. *J. Comp. Phys.*, **20** (4), pp. 397-431.

[8] Casper J. and Atkins H. (1993). A finite-volume high order ENO scheme for two dimensional hyperbolic systems. *J. Comp. Phys.*, **106**, pp. 62-76.

[9] Cockburn B., Lin S.-Y. and Shu C.-W. (1989). TVB Runge-Kutta local projection discontinuous Galerkin finite element method for conservation laws III: one dimensional systems. *J. Comp. Phys.*, **84**, pp.90-113.

[10] Cockburn B. and Shu C.-W. (1998). The Runge-Kutta discontinuous Galerkin method for conservation laws V: multidimensional systems. *J. Comp. Phys.*, **141**, pp.199-224.

[11] Cockburn B. and Shu C.-W. (2001) Runge-Kutta discontinuous Galerkin methods for convection-dominated problems. *J. Sci. Comput.*, **16** , pp. 173-261.

[12] Colella P. (1985). A Direct Eulerian MUSCL Scheme for Gas Dynamics. *SIAM J. Sci. Stat. Comput.*, **6**, pp. 104-117.

[13] Engquist E. and Osher S. (1981). One sided difference approximations for nonlinear conservation laws. *Math. Comp.*, **36** (154), pp. 321-353.

[14] Godunov S. K. (1959). A finite difference method for the computation of discontinious solutions of the equation of fluid dynamics. *Mat. Sb.*, **47**, pp. 357-393.

[15] Godunov S.K., Zabrodin A.V., Ivanov M.Y., Kraiko A.N. and Prokopov G.P. *Numerical solution of multi-dimensional problems in gas dynamics.* Nauka Press, Moscow, 1976 (in Russian).

[16] Godunov S., Zabrodin A. , Ivanov M.Y., Kraiko A.N. and Prokopov G.P. *Resolution Numerique des Problemes Multidimensionnels de la Dinamique des Gaz*, Moscow; Mir 1979. 414 p.

[17] Gurski K.F. (2002). An HLLC approximate Riemann solver for ideal magnetohydrodynamics, submitted for publication.

[18] Jiang G.S. and Shu C.W. (1996). Efficient implementation of weighted ENO schemes. *J. Comput. Phys.*, **126**, pp. 202-212.

[19] Harten A. (1983). High Resolution Schemes for Hyperbolic Conservation Laws. *J.Comp. Phys.*, **49**, pp. 357-393.

[20] Harten A., Engquist B., Osher S. and Chakravarthy S.R. (1987). Uniformly high order accurate essentially non-oscillatory schemes III. *J. Comput. Phys.*, **71** , pp. 231-303.

[21] Harten A. , Lax P. D. and van Leer B. (1983). On upstream differencing and Godunov-type schemes for hyperbolic conservation laws. *SIAM Review*, **25**(1), pp. 35-61.

[22] Hu C. and Shu C.-W. (1999). Weighted essentially non-oscillatory schemes on triangular meshes. *J. Comp. Phys.*, **150**, pp.97-127.

[23] Kolgan N.E. (1972). Application of the minimum-derivative principle in the construction of finite-difference schemes for numerical analysis of discontinuous solutions in gas dynamics. *Uchenye Zapiski TsaGI* [Sci. Notes of Central Inst. of Aerodynamics], **3**(6), pp. 68-77 (in Russian).

[24] Kolgan N.E. (1975). Finite-difference schemes for computation of two dimensional discontinuous solutions of nonstationary gas dynamics. *Uchenye Zapiski TsaGI* [Sci. Notes of Central Inst. of Aerodynamics], **6**(1), pp. 9-14 (in Russian).

[25] Kolgan N.E. (1975). Finite-difference schemes for computation of three dimensional solutions of gas dynamics and calculation of a flow over a body under an angle of attack. *Uchenye Zapiski TsaGI* [Sci. Notes of Central Inst. of Aerodynamics], **6**(2), pp. 1-6 (in Russian).

[26] Kurganov A. and Petrova G. (2000). Central schemes and contact discontinuities. *Mathematical Modelling and Numerical Analysis*, **34**, pp 1259-1275.

[27] Lax P.D. (1954). Weak solutions of nonlinear hyperbolic equations and their numerical computation. *Comm. Pure. Appl. Math.*, **7**, pp. 159-193.

[28] LeVeque R.J. Numerical Methods for Conservation Laws. Birkhauser Verlag, 1992.

[29] Levy D., Puppo G. and Russo G. (1999). Central WENO schemes for hyperbolic systems of conservation laws. *Mathematical Modelling and Numerical Anaysis* **33**, pp. 547-571.

[30] Liu X.D. and Osher S. and Chan T. (1994). Weighted essentially non-oscillatory schemes. *J. Comput. Phys.*, **115**, pp. 200-212.

[31] Nessyahu H. and Tadmor E. (1990). Non-oscillatory central differencing for hyperbolic conservation laws. *J. Comp. Phys.*, **87**, pp. 408-463.

[32] Osher S. and Solomon F. (1982). Upwind difference schemes for hyperbolic conservation laws. *Math. Comp.*, **38**, pp. 339-374.

[33] Qiu J. and Shu C.-W. (2002). On the construction, comparison, and local characteristic decomposition for high order central WENO schemes. *J. Comp. Phys.*, *to appear* .

[34] Roe P.L. (1981). Approximate Riemann solvers, parameter vectors, and difference schemes. *J. Comp. Phys.*, **43**, pp 357-372.

[35] Roe P.L. (1985). Some contributions to the modelling of discontinuous flows. *Lect. Appl. Math.*, **22**.

[36] Rusanov V.V. (1961). Calculation of interaction of non-steady shock waves with obstacles. *USSR J. Comp. Math. Phys.*, **1**, pp. 267-279.

[37] Schwartzkopff T., Munz C.D., Toro E.F. and Millington R.C. (2002). ADER-2D: a high-order approach for linear hyperbolic systems in 2D. *J. Sci. Comput.*, **17**, pp. 231-240.

[38] Shi J., Hu C. and Shu C.-W. (2002). A technique for treating negative weights in WENO schemes. *J. Comp. Phys.*, **175**, pp.108-127.

[39] Shu C.-W. (1988). Total-Variation-Diminishing time discretizations. *SIAM J. Sci. Stat. Comp.*, **9**, pp.1073-1084.

[40] Shu C.-W. and Osher S. (1989). Efficient implementation of essentially non-oscillatory shock capturing schemes II. *J. Comp. Phys.*, **83**, pp.32-78.

[41] Suresh A. and Huynh T. (1997). Accurate monotonicity preserving scheme with Runge-Kutta time stepping. *J. Comp. Phys*, **136**, pp. 83-99.

[42] Sweby P.K. (1984). High Resolution Schemes Using Flux Limiters for Hyperbolic Conservation Laws. *SIAM J. Numer. Anal.*, **21**, pp 995-1011.

[43] Takakura Y. and Toro E.F. (2002). Arbitrarily accurate non-oscillatory schemes for a nonlinear conservation law. *CFD Journal*, **11**(1), pp. 7-18.

[44] Titarev V.A. (2001). *Very High Order ADER Schemes for Nonlinear Conservation Laws*. Department of Computing and Mathematics, Manchester Metropolitan University, UK, MSc. Thesis.

[45] Titarev V.A. and Toro E.F. (2002). ADER: Arbitrary High Order Godunov Approach. *J. Sci. Comput.*, **17**, pp. 609-618.

[46] Titarev V.A. and Toro E.F. (2003). High-Order ADER for the Scalar Advection-Reaction-Diffusion Equations. *CDF Journal, to appear.*

[47] Toro E.F. (1991). *Some aspects of shock capturing methods for gas dynamics* CoA report 9112, August 1991, Department of Aerospace Science, Cranfield Institute of Technology.

[48] Toro E.F. (1996). On Glimm-related schemes for conservation laws. Technical Report MMU-9602, Department of Mathematics and Physics, Manchester Metropolitan University, UK.

[49] Chen G.-Q. and Toro E.F. (2003). Centred Schemes for Nonlinear Hyperbolic Equations. Preprint. Isaac Newton Institute for Mathematical Sciences, University of Cambridge, UK; *to appear*

[50] Toro E. F. and Billett S. J. (2000). Centred TVD Schemes for Hyperbolic Conservation Laws. *IMA J. Numerical Analysis*, **20**, pp 47-79.

[51] Toro E.F. (1999). *Riemann Solvers and Numerical Methods for Fluid Dynamics*. Second Edition, Springer-Verlag.

[52] Toro E.F. (1989). A Weighted Average Flux Method for Hyperbolic Conservation Laws. *Proceedings of the Royal Society of London*, A 423, pp 401-418.

[53] Toro E.F. (1992). The Weighted Average Flux Method Applied to the Euler Equations. *Phil. Trans. of the Royal Society of London*, A 341, pp 499-530.

[54] Toro E.F., Millington R. C. and Nejad L. A. M. (2001). Towards Very High Order Godunov Schemes. In:*Godunov Methods. Theory and Applications*, Edited Review, E. F. Toro (Editor), Kluwer/Plenum Academic Publishers, pp 907-940.

[55] Toro E.F., Spruce M. and Speares W. (1994). Restoration of the Contact Surface in the Harten-Lax-van Leer Riemann Solver. CoA report 9204, January 1992, Department of Aerospace Science, Cranfield Institute of Technology.

[56] Toro E.F., Spruce M. and Speares W. (1994). Restoration of the Contact Surface in the Harten-Lax-van Leer Riemann Solver. *Journal of Shock Waves*, **4**, pp. 25-34.

[57] Toro E.F. and Titarev V. A. (2002). Solution of the Generalised Riemann Problem for Advection-Reaction Equations. *Proc. Roy. Soc. London*, **458**, N2018, pp. 271-281.

[58] Toro E.F. and Titarev V.A. (2003). TVD Fluxes for the High-Order ADER Schemes. Preprint NI03011-NPA. Isaac Newton Institute for Mathematical Sciences, University of Cambridge, UK. 16 April 2003; submitted to *J. Sci. Comput.*

[59] Toro E.F. and Titarev V.A. (2001). The ADER approach for nonlinear advection-diffusion-reaction equations. In: *The 8th National Conference on Computational Fluid Dynamics*, E-Land, Taiwan, August 18-20, 2001.

[60] van Leer B. (1973). Towards the ultimate conservative difference scheme I: the quest for monotonicity. *Lecture Notes in Physics* **18**, pp. 163-168.

[61] van Leer B. (1979). Towards the ultimate conservative difference Scheme V: a second order sequel to Godunov' method. *J. Comput. Phys.* **32**, pp. 101-136.

[62] van der Vegt J.J.W. and van der Ven H. (2001). Space-time discontinuous Galerkin Finite Element method with Dynamic Grid motion for inviscid Compressible flows 1. General formulation, submitted to *J. Comp. Phys.*

[63] van der Ven H. and van der Vegt J.J.W (2002). Space-time discontinuous Galerkin Finite Element method with Dynamic Grid motion for inviscid Compressible flows 2. Efficient Flux Quadrature. submitted to *J. Comp. Phys.*

[64] Zhou T., Li Y. and Shu C.W. (2001). Numerical Comparison of WENO finite volume and Runge-Kutta Discontinuous Galerkin Methods. *J. Sci. Comp.*, **16** (2), pp 145-171.

[65] Woodrwad P. and Colella P. (1984). The piece-wise parabolic method (PPM) for gas-dynamical simulations. *J. Comp. Phys.*, **54** pp. 174-201.

Table 1: Convergence study for various schemes as applied to the model equation (37) with initial condition (38) at output time $t = 1$. Schemes: second order WAF and FLIC used with CFL=0.95 and spatially fifth order WENO and WENO-TVD used with CFL=0.4.

Method	N	L_∞ error	L_∞ order	L_1 error	L_1 order
FLIC	20	1.17×10^{-1}		7.33×10^{-2}	
	40	3.81×10^{-2}	1.62	2.27×10^{-2}	1.69
	80	1.59×10^{-2}	1.26	6.04×10^{-3}	1.91
	160	6.44×10^{-3}	1.31	1.54×10^{-3}	1.97
	320	2.59×10^{-3}	1.32	3.87×10^{-4}	1.99
	640	1.03×10^{-3}	1.33	9.49×10^{-5}	2.03
WAF	20	4.74×10^{-2}		3.46×10^{-2}	
	40	1.84×10^{-2}	1.36	6.73×10^{-3}	2.36
	80	7.67×10^{-3}	1.26	1.92×10^{-3}	1.81
	160	3.10×10^{-3}	1.31	4.84×10^{-4}	1.99
	320	1.22×10^{-3}	1.34	1.15×10^{-4}	2.07
	640	4.75×10^{-4}	1.37	2.92×10^{-5}	1.98
WENO-LF	20	1.64×10^{-1}		1.49×10^{-1}	
	40	1.61×10^{-2}	3.35	1.64×10^{-2}	3.19
	80	2.11×10^{-3}	2.93	1.79×10^{-3}	3.20
	160	1.09×10^{-4}	4.27	7.32×10^{-5}	4.61
	320	3.66×10^{-6}	4.90	3.47×10^{-6}	4.40
	640	3.51×10^{-7}	3.39	3.31×10^{-7}	3.48
WENO-HLLC	20	1.22×10^{-1}		1.05×10^{-1}	
	40	8.84×10^{-3}	3.78	8.00×10^{-3}	3.72
	80	1.49×10^{-3}	2.57	9.81×10^{-4}	3.03
	160	5.64×10^{-5}	4.72	4.18×10^{-5}	4.55
	320	3.00×10^{-6}	4.23	2.80×10^{-6}	3.90
	640	3.29×10^{-7}	3.19	3.29×10^{-7}	3.09
WENO-FLIC	20	1.21×10^{-1}		1.07×10^{-1}	
	40	8.98×10^{-3}	3.75	7.12×10^{-3}	3.91
	80	1.48×10^{-3}	2.60	7.81×10^{-4}	3.19
	160	3.29×10^{-5}	5.49	2.84×10^{-5}	4.78
	320	2.74×10^{-6}	3.59	2.62×10^{-6}	3.44
	640	3.22×10^{-7}	3.09	3.28×10^{-7}	3.00
WENO-WAF	20	6.98×10^{-2}		6.52×10^{-2}	
	40	6.18×10^{-3}	3.50	6.27×10^{-3}	3.38
	80	1.10×10^{-3}	2.49	6.44×10^{-4}	3.28
	160	3.41×10^{-5}	5.01	3.02×10^{-5}	4.42
	320	2.77×10^{-6}	3.62	2.61×10^{-6}	3.53
	640	3.22×10^{-7}	3.09	3.28×10^{-7}	3.00

Table 2: Convergence study for various schemes as applied to the model equation (37) with initial condition (38) at output time $t = 1000$. Schemes: second order WAF and FLIC used with CFL=0.95 and spatially fifth order WENO and WENO-TVD used with CFL=0.4.

Method	N	L_∞ error	L_∞ order	L_1 error	L_1 order
FLIC	20	5.62×10^{-1}		6.52×10^{-1}	
	40	6.09×10^{-1}	-0.11	6.52×10^{-1}	0.00
	80	6.17×10^{-1}	-0.02	6.47×10^{-1}	0.01
	160	4.07×10^{-1}	0.60	4.05×10^{-1}	0.67
	320	1.94×10^{-1}	1.07	1.65×10^{-1}	1.30
	640	8.34×10^{-2}	1.22	6.07×10^{-2}	1.44
WAF	20	5.77×10^{-1}		6.66×10^{-1}	
	40	6.05×10^{-1}	-0.07	6.47×10^{-1}	0.04
	80	3.89×10^{-1}	0.64	3.58×10^{-1}	0.85
	160	1.68×10^{-1}	1.21	1.22×10^{-1}	1.55
	320	7.04×10^{-2}	1.25	5.05×10^{-2}	1.28
	640	2.56×10^{-2}	1.46	1.53×10^{-2}	1.72
WENO-LF	20	5.62×10^{-1}		6.52×10^{-1}	
	40	6.05×10^{-1}	-0.11	6.47×10^{-1}	0.01
	80	3.29×10^{-1}	0.88	3.05×10^{-1}	1.09
	160	4.17×10^{-1}	-0.34	4.10×10^{-1}	-0.43
	320	3.54×10^{-3}	6.88	2.86×10^{-3}	7.16
	640	3.48×10^{-4}	3.35	3.31×10^{-4}	3.30
WENO-HLLC	20	5.62×10^{-1}		6.52×10^{-1}	
	40	5.68×10^{-1}	-0.01	6.00×10^{-1}	0.12
	80	2.10×10^{-1}	1.44	1.74×10^{-1}	1.79
	160	8.49×10^{-2}	1.30	5.66×10^{-2}	1.62
	320	2.93×10^{-3}	4.86	2.59×10^{-3}	4.45
	640	3.29×10^{-4}	3.15	3.29×10^{-4}	2.98
WENO-FLIC	20	5.62×10^{-1}		6.52×10^{-1}	
	40	4.98×10^{-1}	0.17	5.13×10^{-1}	0.35
	80	1.57×10^{-1}	1.67	1.34×10^{-1}	1.94
	160	2.38×10^{-2}	2.72	1.82×10^{-2}	2.88
	320	2.68×10^{-3}	3.15	2.60×10^{-3}	2.81
	640	3.22×10^{-4}	3.06	3.28×10^{-4}	2.98
WENO-WAF	20	5.62×10^{-1}		6.52×10^{-1}	
	40	4.68×10^{-1}	0.27	4.78×10^{-1}	0.45
	80	1.51×10^{-1}	1.63	1.34×10^{-1}	1.83
	160	2.37×10^{-2}	2.67	1.86×10^{-2}	2.85
	320	2.69×10^{-3}	3.14	2.54×10^{-3}	2.87
	640	3.22×10^{-4}	3.06	3.28×10^{-4}	2.98

Table 3: Convergence study for various schemes as applied to the model equation (37) with initial condition (39) at output times $t = 20$ and $t = 2000$. Schemes: second order TVD FLIC and WAF used with CFL=0.95 and spatially fifth order WENO and WENO-TVD used with CFL=0.4.

Scheme	N	$t = 20$		$t = 2000$	
FLIC	200	1.92×10^{-1}		6.19×10^{-1}	
	400	1.03×10^{-1}	0.90	5.78×10^{-1}	0.10
	800	5.50×10^{-2}	0.90	4.13×10^{-1}	0.48
	1600	2.90×10^{-2}	0.92	2.36×10^{-1}	0.81
WAF	200	1.00×10^{-1}		5.52×10^{-1}	
	400	5.27×10^{-2}	0.93	3.47×10^{-1}	0.67
	800	2.68×10^{-2}	0.98	1.86×10^{-1}	0.90
	1600	1.43×10^{-2}	0.90	9.81×10^{-2}	0.93
WENO-LF	200	1.42×10^{-1}		6.41×10^{-1}	
	400	6.86×10^{-2}	1.05	6.21×10^{-1}	0.05
	800	4.12×10^{-2}	0.76	5.82×10^{-1}	0.09
	1600	3.06×10^{-2}	0.43	5.18×10^{-1}	0.17
WENO-HLLC	200	1.13×10^{-1}		4.16×10^{-1}	
	400	4.95×10^{-2}	1.19	4.00×10^{-1}	0.06
	800	2.34×10^{-2}	1.08	3.28×10^{-1}	0.29
	1600	1.26×10^{-2}	0.89	1.66×10^{-1}	0.98
WENO-FLIC	200	9.53×10^{-2}		3.26×10^{-1}	
	400	4.16×10^{-2}	1.20	1.74×10^{-1}	0.91
	800	1.97×10^{-2}	1.08	9.10×10^{-2}	0.93
	1600	1.02×10^{-2}	0.95	5.03×10^{-2}	0.86
WENO-WAF	200	8.76×10^{-2}		3.12×10^{-1}	
	400	3.95×10^{-2}	1.15	1.55×10^{-1}	1.01
	800	1.90×10^{-2}	1.06	8.52×10^{-2}	0.86
	1600	9.90×10^{-3}	0.94	4.55×10^{-2}	0.90

Table 4: Convergence study for various schemes as applied to the Euler equations (21) with initial condition (40). Schemes: FLIC and WAF used with CFL=0.95, ENO and WENO used with CFL=0.4 an MPWENO used with CFL=0.3.

Scheme	N. of time steps	L_1 error	N. of cells across the discontinuity
FLIC	1	0	0
WAF	1	0	0
ENO-LF	2134	3.69×10^{-3}	35
ENO-HLLC	1	0	0
ENO-FLIC	1	0	0
ENO-WAF	1	0	0
WENO-LF	1482	3.48×10^{-3}	20
WENO-HLLC	1	0	0
WENO-FLIC	1	0	0
WENO-WAF	1	0	0
MPWENO-LF	1109	3.06×10^{-3}	8
MPWENO-HLLC	1	0	0
MPWENO-FLIC	1	0	0
MPWENO-WAF	1	0	0

Table 5: Computing times of various schemes as applied to the Euler equations (21) with initial condition (41) on the mesh of 2000 cells.

Scheme	CFL number	Computing time
FLIC	0.95	5s
WAF	0.95	5s
WENO-LF	0.4	52s
WENO-HLLC	0.4	60s
WENO-FLIC	0.4	58s
WENO-WAF	0.4	80s
MPWENO-LF	0.3	172s
MPWENO-FLIC	0.3	180s
MPWENO-HLLC	0.3	182s
MPWENO-WAF	0.3	212s

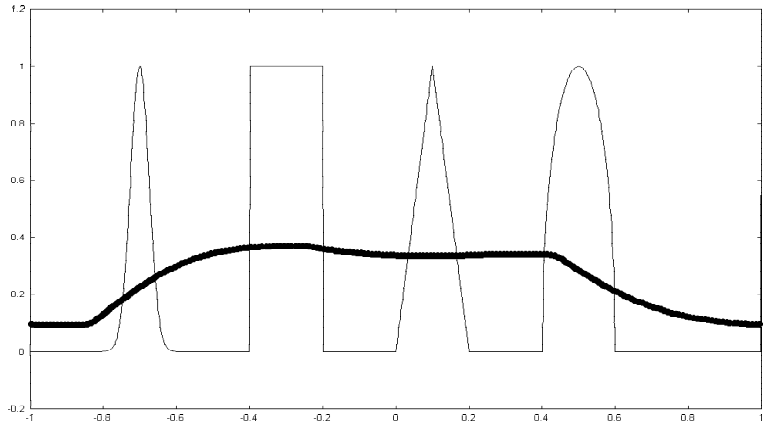

Figure 1: Computed (symbols) and exact (line) solutions for equation (37) with initial condition (39) at output $t = 2000$. Method used: second order TVD FLIC, CFL=0.95 and N=200.

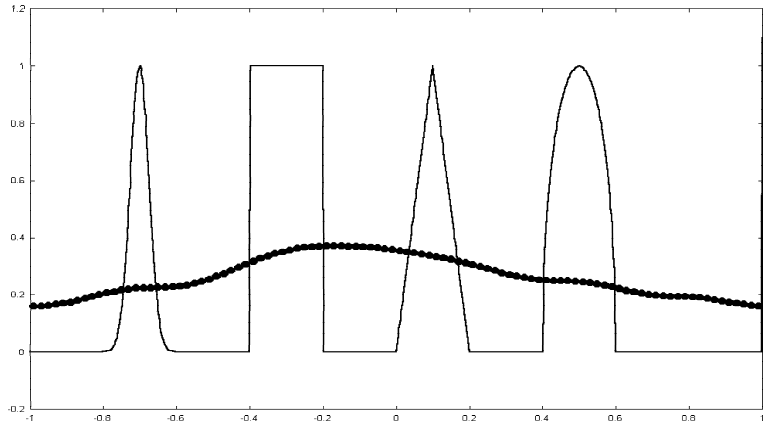

Figure 2: Computed (symbols) and exact (line) solutions for equation (37) with initial condition (39) at output $t = 2000$. Method used: spatially fifth order WENO-LF, CFL=0.4 and N=200.

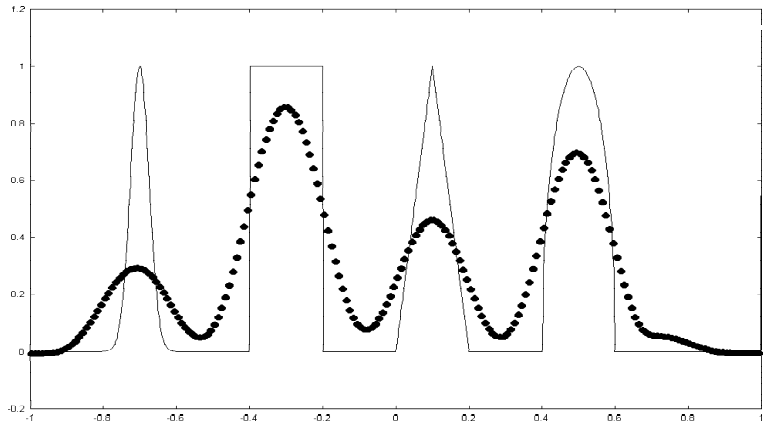

Figure 3: Computed (symbols) and exact (line) solutions for equation (37) with initial condition (39) at output $t = 2000$. Method used: spatially fifth order WENO-FLIC, CFL=0.4 and N=200.

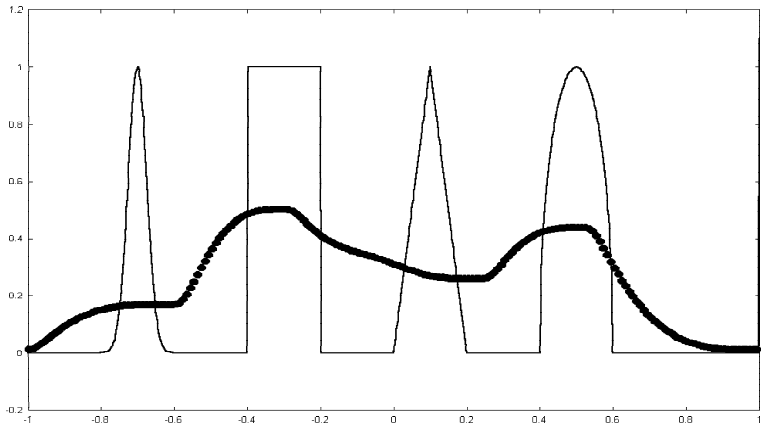

Figure 4: Computed (symbols) and exact (line) solutions for equation (37) with initial condition (39) at output $t = 2000$. Method used: second order TVD WAF, CFL=0.95 and N=200.

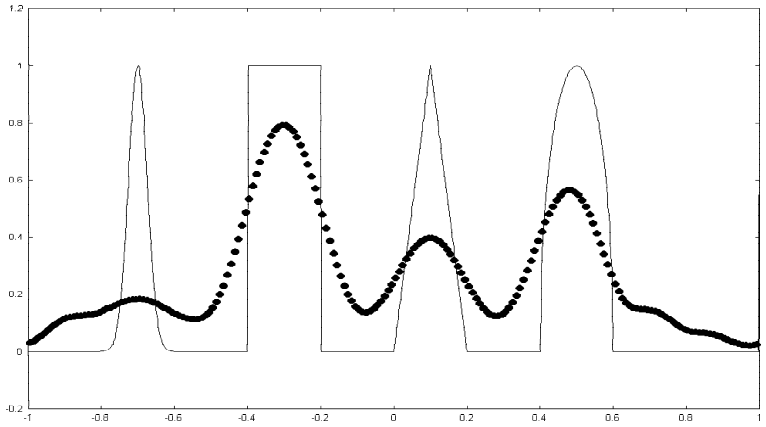

Figure 5: Computed (symbols) and exact (line) solutions for the linear advection equation (37) with initial condition (39) at output $t = 2000$. Method used: spatially fifth order WENO-HLLC, CFL=0.4 and N=200.

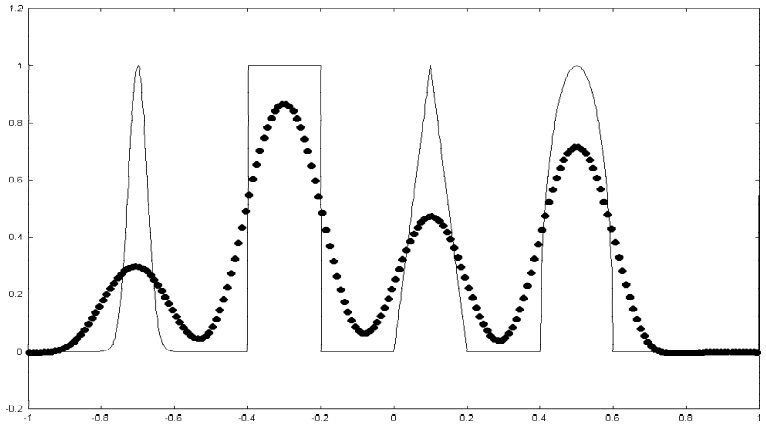

Figure 6: Computed (symbols) and exact (line) solutions for the linear advection equation (37) with initial condition (39) at output $t = 2000$. Method used: spatially fifth order WENO-WAF, CFL=0.4 and N=200.

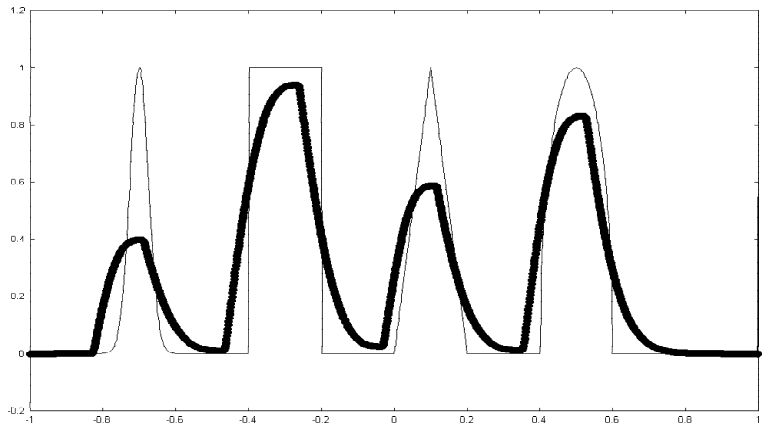

Figure 7: Computed (symbols) and exact (line) solutions for equation (37) with initial condition (39) at output $t = 2000$. Method used: second order TVD FLIC, CFL=0.95 and N=1600.

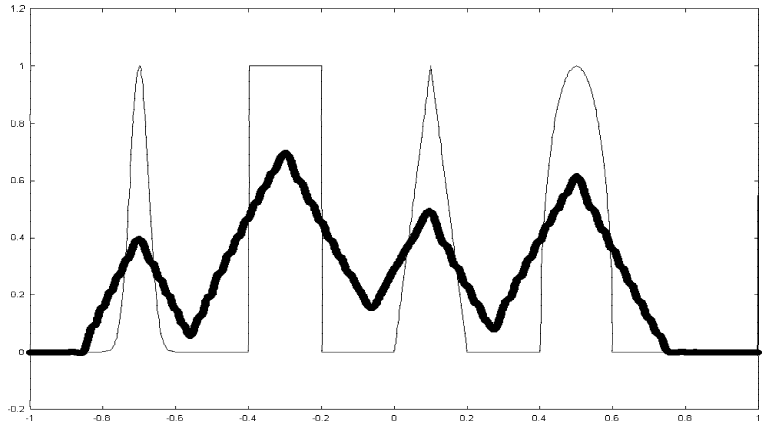

Figure 8: Computed (symbols) and exact (line) solutions for equation (37) with initial condition (39) at output $t = 2000$. Method used: spatially fifth order WENO-LF, CFL=0.4 and N=1600.

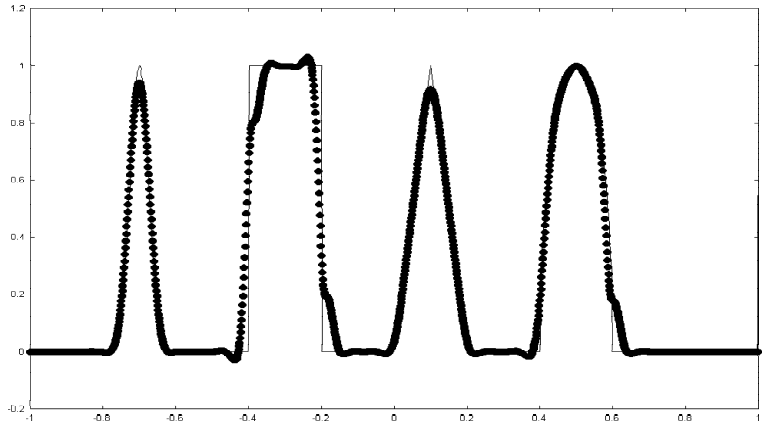

Figure 9: Computed (symbols) and exact (line) solutions for equation (37) with initial condition (39) at output $t = 2000$. Method used: spatially fifth order WENO-FLIC, CFL=0.4 and N=1600.

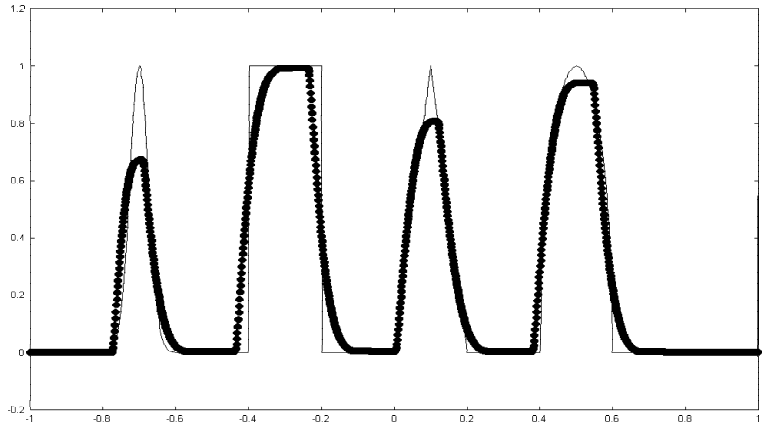

Figure 10: Computed (symbols) and exact (line) solutions for equation (37) with initial condition (39) at output $t = 2000$. Method used: second order TVD WAF, CFL=0.95 and N=1600.

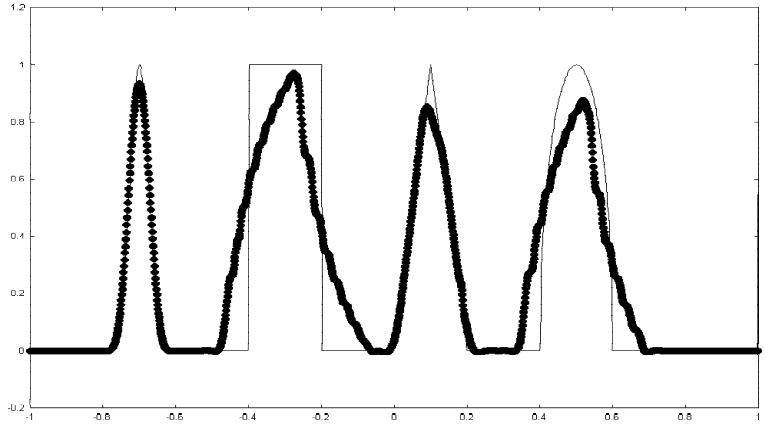

Figure 11: Computed (symbols) and exact (line) solutions for the linear advection equation (37) with initial condition (39) at output $t = 2000$. Method used: fifth order WENO-HLLC, CFL=0.4 and N=1600.

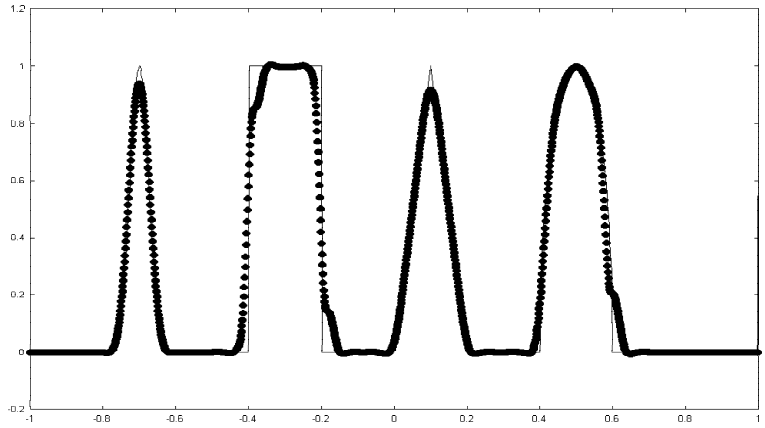

Figure 12: Computed (symbols) and exact (line) solutions for the linear advection equation (37) with initial condition (39) at output $t = 2000$. Method used: spatially fifth order WENO-WAF, CFL=0.4 and N=1600.

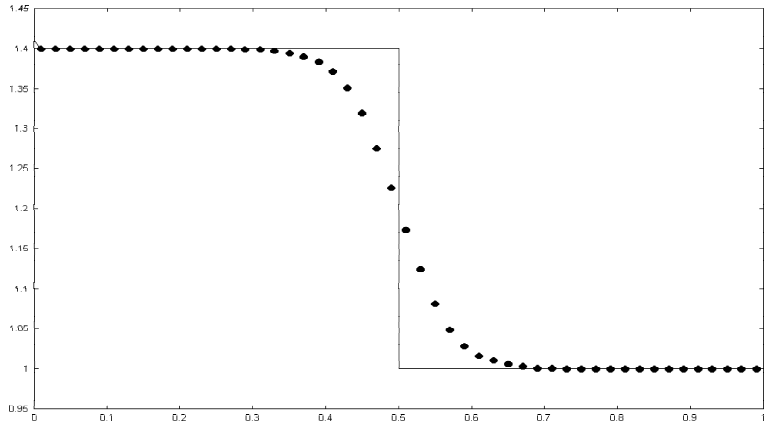

Figure 13: Computed (symbol) and reference (line) solutions for the Euler equations (21) with initial condition (40). Method used: fifth order WENO-LF, CFL=0.4 and N=50 cells.

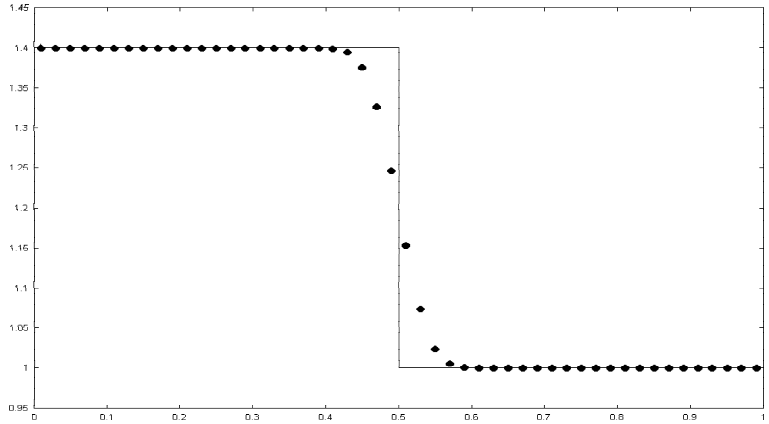

Figure 14: Computed (symbol) and reference (line) solutions for the Euler equations (21) with initial condition (40). Method used: ninth order MPWENO-LF, CFL=0.3 and N=50 cells.

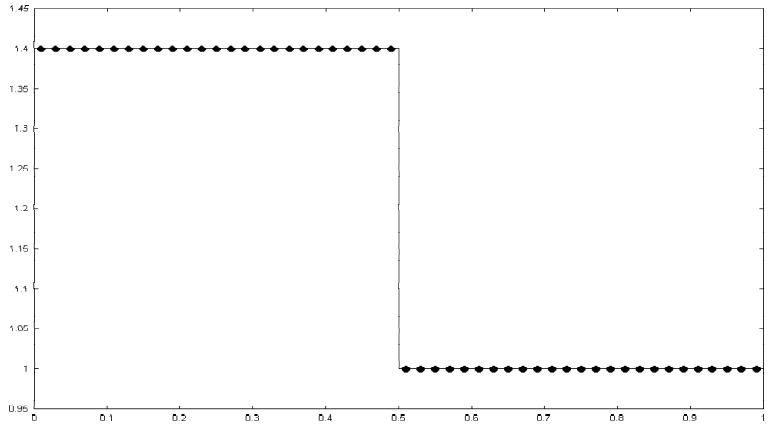

Figure 15: Computed (symbol) and reference (line) solutions for the Euler equations (21) with initial condition (40). Method used: fifth order ENO-FLIC, CFL=0.4 and N=50 cells.

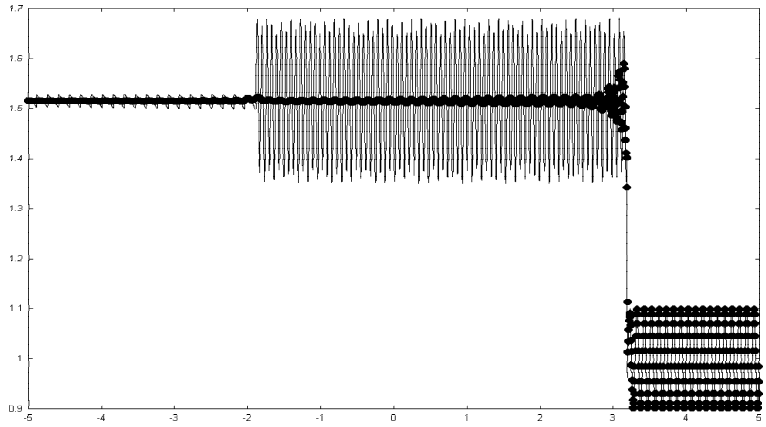

Figure 16: Computed (symbol) and reference (line) solutions for the Euler equations (21) with initial condition (41) at output time $t = 5$. Method used: second order TVD FLIC, CFL=0.95 and N=2000 cells.

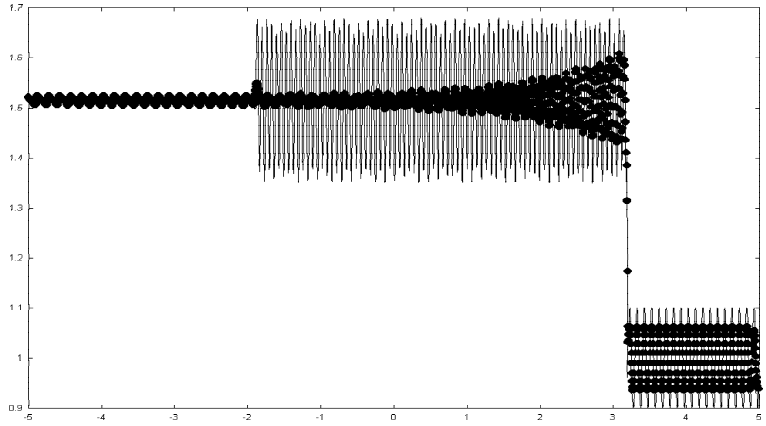

Figure 17: Computed and reference (line) solutions for the Euler equations (21) with initial condition (41) at output time $t = 5$. Method used: spatially fifth order WENO-LF, CFL=0.4 and N=2000 cells.

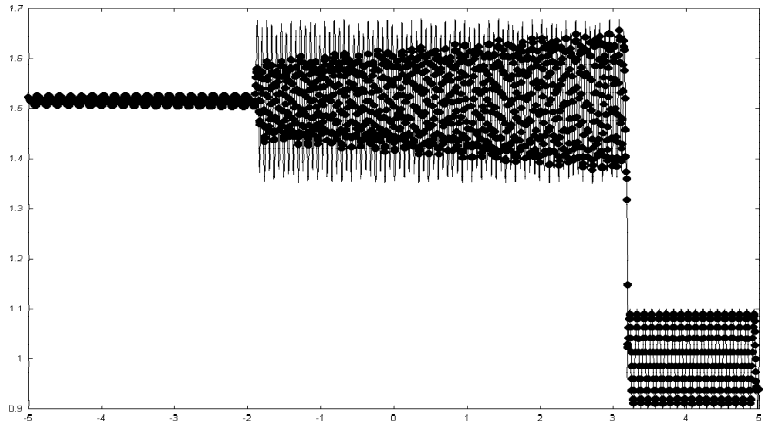

Figure 18: Computed and reference (line) solutions for the Euler equations (21) with initial condition (41) at output time $t = 5$. Method used: spatially fifth order WENO-FLIC, CFL=0.4 and N=2000 cells.

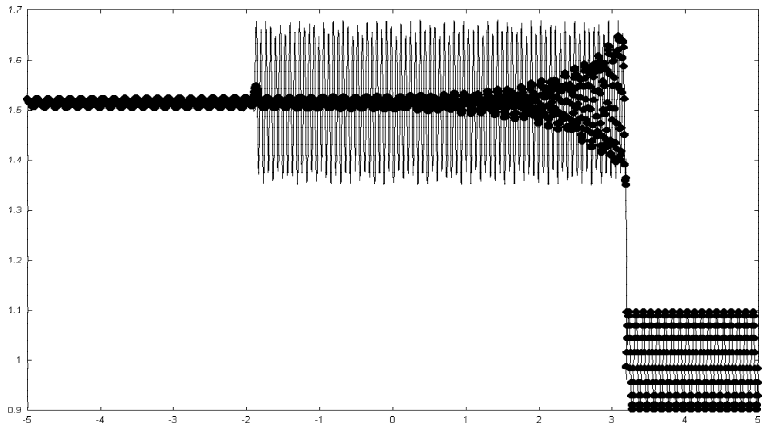

Figure 19: Computed (symbol) and reference (line) solutions for the Euler equations (21) with initial condition (41) at output time $t = 5$. Method used: second order TVD WAF, CFL=0.95 and N=2000 cells.

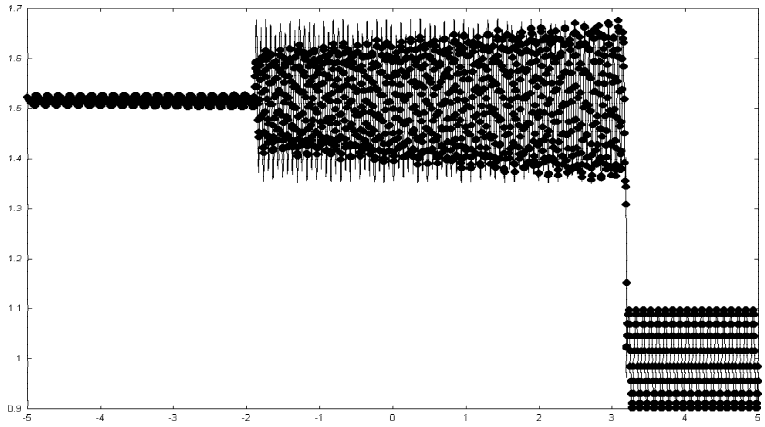

Figure 20: Computed (symbol) and reference (line) solutions for the Euler equations (21) with initial condition (41) at output time $t = 5$. Method used: spatially fifth order WENO-HLLC, CFL=0.4 and N=2000 cells.

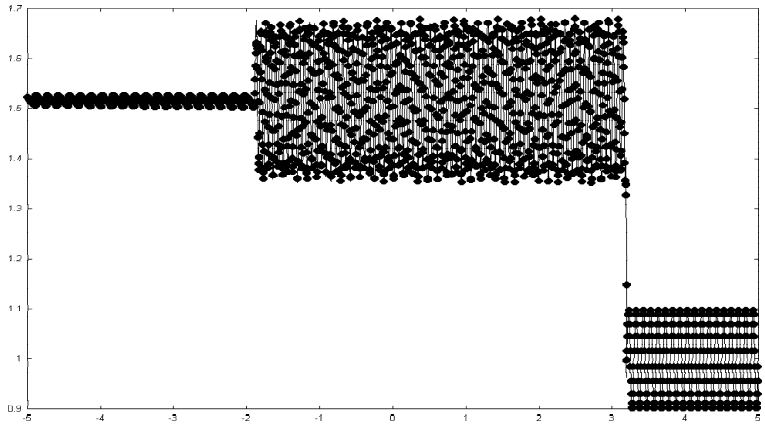

Figure 21: Computed (symbol) and reference (line) solutions for the Euler equations (21) with initial condition (41) at output time $t = 5$. Method used: spatially fifth order WENO-WAF, CFL=0.4 and N=2000 cells.

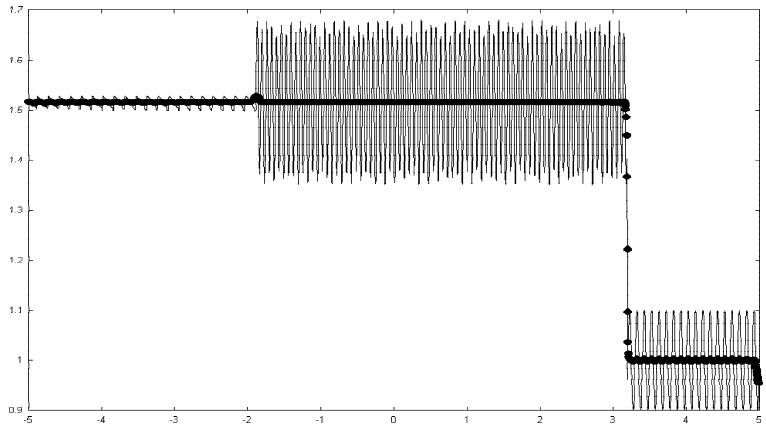

Figure 22: Computed (symbol) and reference (line) solutions for the Euler equations (21) with initial condition (41) at output time $t = 5$. Method used: spatially third order ENO-LF, CFL=0.4 and N=2000 cells.

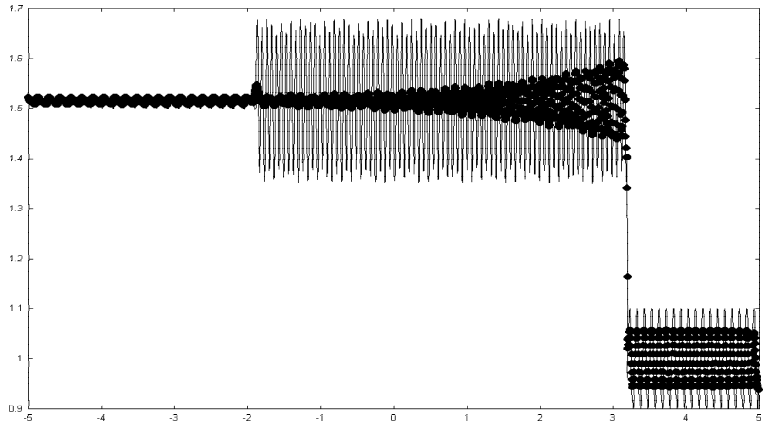

Figure 23: Computed (symbol) and reference (line) solutions for the Euler equations (21) with initial condition (41) at output time $t = 5$. Method used: spatially third order ENO-FLIC, CFL=0.4 and N=2000 cells.

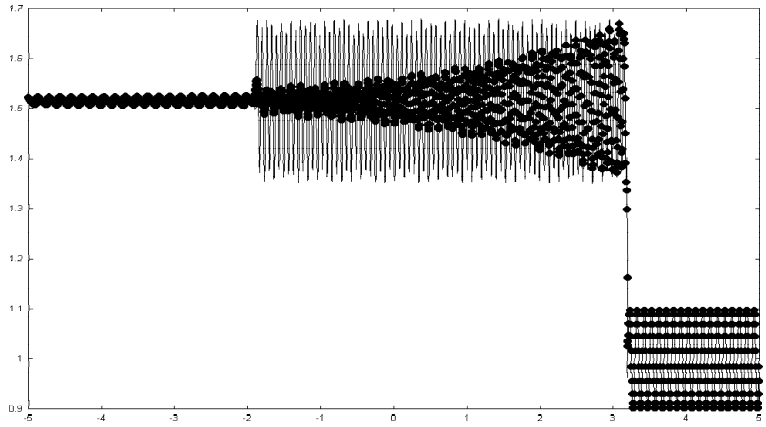

Figure 24: Computed (symbol) and reference (line) solutions for the Euler equations (21) with initial condition (41) at output time $t = 5$. Method used: spatially third order ENO-HLLC, CFL=0.4 and N=2000 cells.

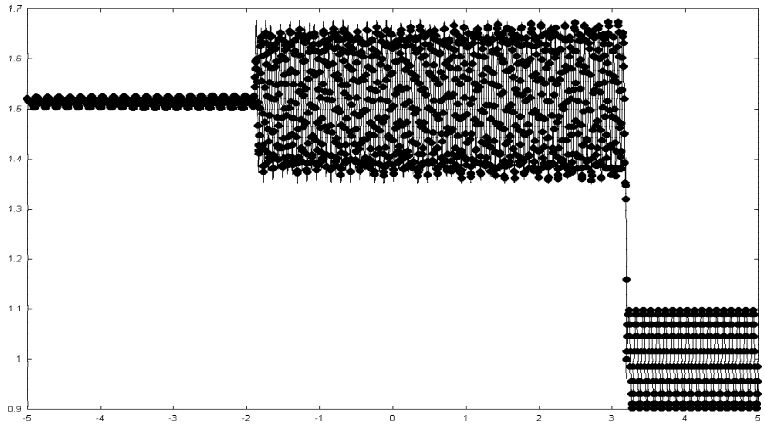

Figure 25: Computed (symbol) and reference (line) solutions for the Euler equations (21) with initial condition (41) at output time $t = 5$. Method used: spatially third order ENO-WAF, CFL=0.4 and N=2000 cells.

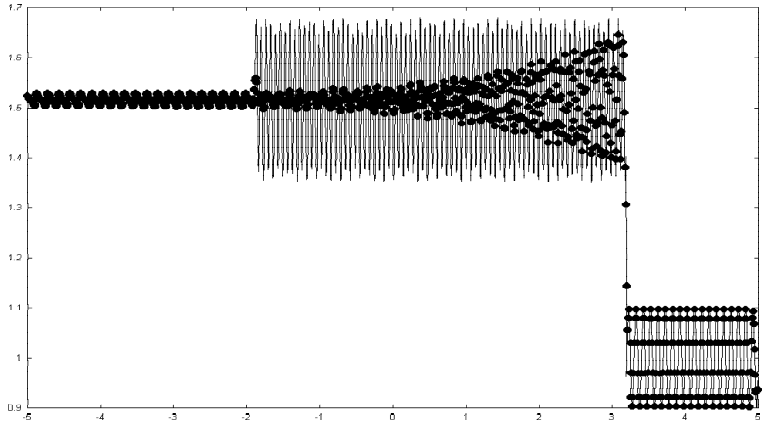

Figure 26: Computed (symbol) and reference (line) solutions for the Euler equations (21) with initial condition (41) at output time $t = 5$. Method used: spatially ninth order MPWENO-LF, CFL=0.3 and N=1000 cells.

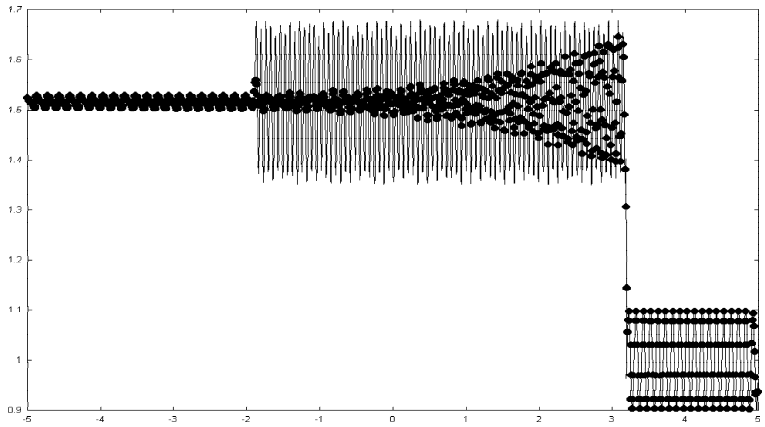

Figure 27: Computed (symbol) and reference (line) solutions for the Euler equations (21) with initial condition (41) at output time $t = 5$. Method used: spatially ninth order MPWENO-FLIC, CFL=0.3 and N=1000 cells.

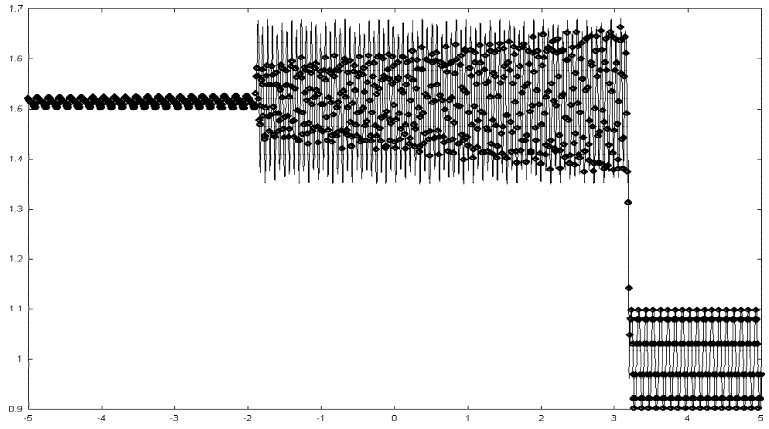

Figure 28: Computed (symbol) and reference (line) solutions for the Euler equations (21) with initial condition (41) at output time $t = 5$. Method used: spatially ninth order MPWENO-HLLC, CFL=0.3 and N=1000 cells.

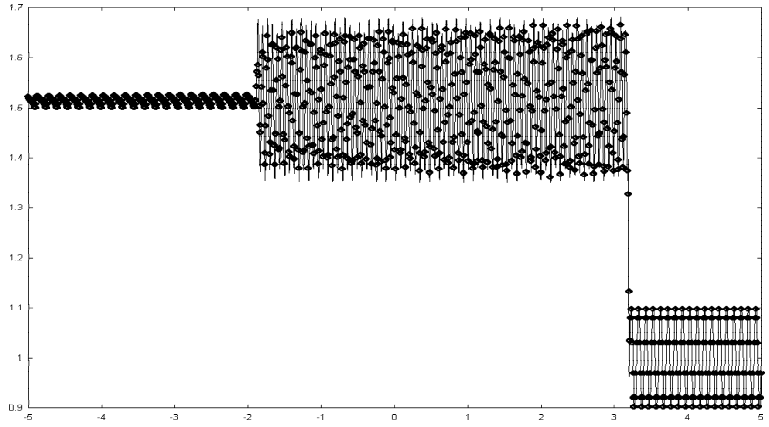

Figure 29: Computed (symbol) and reference (line) solutions for the Euler equations (21) with initial condition (41) at output time $t = 5$. Method used: spatially ninth order MPWENO-WAF, CFL=0.3 and N=1000 cells.